SR-B1 Drives Endothelial Cell LDL Transcytosis via DOCK4 to Promote Atherosclerosis

Linzhang Huang[1], **Ken L. Chambliss**[1], **Xiaofei Gao**[2,3], **Ivan S. Yuhanna**[1], **Erica Behling-Kelly**[1,†], **Sonia Bergaya**[4], **Mohamed Ahmed**[1], **Peter Michaely**[5], **Kate Luby-Phelps**[5], **Anza Darehshouri**[5], **Lin Xu**[6], **Edward A. Fisher**[4], **Woo-Ping Ge**[2,3], **Chieko Mineo**[1,5], and **Philip W. Shaul**[1,*]

[1]Center for Pulmonary and Vascular Biology, Department of Pediatrics, University of Texas Southwestern Medical Center,Dallas, TX 75390, USA

[2]Children's Research Institute and Department of Pediatrics, University of Texas Southwestern Medical Center,Dallas, TX 75390, USA

[3]Departments of Neuroscience, and Neurology and Neurotherapeutics, University of Texas Southwestern Medical Center,Dallas, TX 75390, USA

[4]Department of Medicine, Leon H. Charney Division of Cardiology, and the Marc and Ruti Bell Program in Vascular Biology, New York University School of Medicine, New York, NY 10016, USA

[5]Department of Cell Biology, University of Texas Southwestern Medical Center,Dallas, TX 75390, USA

[6]Quantitative Biomedical Research Center, Department of Clinical Sciences, and Department of Pediatrics University of Texas Southwestern Medical Center,Dallas, TX 75390, USA

SUMMARY

Atherosclerosis, which underlies life-threatening cardiovascular disorders including myocardial infarction and stroke[1], is initiated by low density lipoprotein cholesterol (LDL) passage into the artery wall and engulfment by macrophages, leading to foam cell formation and lesion development[2, 2, 3, 3]. How circulating LDL enters the artery wall to instigate atherosclerosis is unknown. Here we show in mice that scavenger receptor, class B type 1 (SR-B1) in endothelial

cells mediates LDL delivery into arteries and its accumulation by artery wall macrophages, thereby promoting atherosclerosis. LDL particles are colocalized with SR-B1 in endothelial cell intracellular vesicles in vivo, and LDL transcytosis across endothelial monolayers requires its direct binding to SR-B1 and an 8 amino acid cytoplasmic domain of the receptor that recruits the guanine nucleotide exchange factor dedicator of cytokinesis 4 (DOCK4)[4]. DOCK4 promotes SR-B1 internalization and LDL transport by coupling LDL binding to SR-B1 with Rac1 activation. SR-B1 and DOCK4 expression are increased in atherosclerosis-prone regions of the mouse aorta prior to lesion formation, and in human atherosclerotic versus normal arteries. These findings challenge the long-held concept that atherogenesis involves passive LDL movement across a compromised endothelial barrier. Interventions inhibiting endothelial delivery of LDL into the artery wall may represent a new therapeutic category in the battle against cardiovascular disease.

In atherosclerosis, the balance of actions of lipoprotein particles governs the severity of the disorder and the likelihood that clinical cardiovascular events will occur. Whereas LDL that enters the artery wall is the critical driver of atherogenesis, via binding to SR-B1 in hepatocytes, high density lipoprotein particles (HDL) mediate reverse cholesterol transport (RCT) to the liver for biliary disposal and are thereby antiatherogenic[5]. In addition, in endothelial cells via SR-B1 and its adaptor PDZK1, HDL stimulates endothelial NO synthase (eNOS)[6], endothelial repair and anti-inflammatory processes which may also be atheroprotective[7]. To determine how SR-B1 in endothelium impacts atherosclerosis, mice lacking the receptor selectively in endothelium were generated (SR-B1 ^{EC}, Extended Data Fig. 1a–i) and placed on apolipoprotein E null (apoE$^{-/-}$) background. To our initial surprise, compared with SR-B1 floxed (SR-B1$^{fl/fl}$) controls, SR-B1 ^{EC} had markedly less atherosclerosis. This was evident in both males and females, and in mice on mixed or C57BL/6 background (Fig. 1a–e, Extended Data Fig. 2a–e,h–l), and it was phenocopied in mice with genetically-induced or PCSK9-induced LDL receptor (LDLR) deficiency (Extended Data Fig. 3a–e, 4a–e), underscoring the robustness of the phenotype. In stark contrast, with selective silencing of SR-B1 in hepatocytes, atherosclerosis was more severe and early deaths occurred related to coronary artery occlusions and fibrotic myocardial lesions (Extended Data Fig. 4m–q), as observed in SR-B1$^{-/-}$;apoE$^{-/-}$ mice[8]. In all models tested the endothelial deletion of SR-B1 which yielded atheroprotection did not alter circulating total cholesterol, triglyceride or HDL levels, or lipoprotein profile (Fig. 1f–i, Extended Data Figs. 2f–g,m–n, 3f–i, and 4f–i). Endothelial SR-B1 also did not impact inflammation-related gene expression in the aorta, or leukocyte-endothelial cell adhesion under basal or TNFα-induced proinflammatory conditions (Extended Data Fig. 5a–k). Importantly, endothelial loss of the SR-B1 adaptor protein PDZK1 (PDZK1 ^{EC}, Extended Data Fig. 1j–o) had no effect on lesion severity (Extended Data Fig. 2o–s). Thus, in marked contrast to its role in hepatocytes, in the absence of impact on circulating lipids or vascular inflammation and independent of processes governed by PDZK1, SR-B1 in endothelium promotes atherosclerosis.

Since SR-B1 is a receptor for both HDL and LDL[9], and in cultured endothelial cells SR-B1 promotes LDL transcytosis[10], the hypothesis was then tested that endothelial SR-B1 influences atherosclerosis by regulating LDL-related processes in the artery wall. DiI-labeled human native LDL (nLDL) transfer into the aorta was visualized in vivo by confocal

fluorescence microscopy. Following IV injection, far less DiI-nLDL entered the aorta of SR-B1 [EC] mice compared to SR-B1^{fl/fl} controls (Fig. 1j–l). Since circulating oxidized LDL (oxLDL) may also contribute to atherogenesis[11, 12], DiI-labeled human oxLDL transfer was also visualized, and it was similarly diminished in SR-B1 [EC] (Extended Data Fig. 6a–c, Videos S1 and S2). Decreased human LDL transfer into the aorta in SR-B1 [EC] was confirmed by quantification in aorta homogenates (Extended Data Fig. 3j–k, 4j–k, 6d–e,j–k), and mouse LDL and IDL/VLDL uptake was also decreased (Extended Data Fig. 3l–m). As such, the prior finding of less LDL accumulation in ex vivo perfused arteries from global SR-B1^{−/−} mice[10] was likely related to loss of the receptor in endothelium. In SR-B1 [EC] mice, Evans blue dye uptake in aorta was unaltered (Fig. 1m), and in mice with intact endothelial SR-B1, anti-SR-B1 blocking antibody treatment lowered aorta LDL incorporation (Extended Data Fig. 6f–g,l–m) and LDL and SR-B1 were colocalized in endothelial cell intracellular vesicles (Fig. 1n, Extended Data Fig. 7). Moreover, whereas FACS studies of CD45+, F4/80+ macrophages indicated no change in their number in the artery wall in SR-B1 [EC], fewer macrophages contained administered LDL (Fig. 1o–p, Extended Data Fig. 5l, 6h–i). These collective observations indicate that endothelial SR-B1 mediates the transcellular transport of LDL from the circulation into the artery wall and the formation of foam cells, thereby promoting atherosclerosis.

The relative importance and mechanistic basis for SR-BI trafficking of LDL was then explored in human aortic endothelial cells (HAEC). Regarding the initial step in LDL transport, whereas SR-B1 knockdown decreased Di-I LDL uptake, PDZK1 ablation had no effect (Extended Data Fig. 8a), as previously observed with HDL[13]. SR-B1 blocking antibody and the chemical SR-B1 inhibitor BLT-1 also attenuated LDL uptake, and either treatment or SR-B1 knockdown blunted LDL transcytosis across endothelial cell monolayers (Extended Data Fig. 8b–d). Whether the loss of SR-B1 impairs the function of endothelial cell caveolae, which mediate LDL transport[14, 15], was assessed in studies of ligand-induced eNOS activation. Whereas SR-B1 silencing predictably negated HDL activation of eNOS[6], stimulation by the eNOS agonist VEGF was unaffected (Extended Data Fig. 8e), paralleling complete loss versus no change in vasodilation with HDL versus acetylcholine in aortic rings from SR-B1^{−/−} mice[6]. In contrast, cyclodextrin disruption of caveolae structure blunted eNOS activation by both VEGF and HDL (Extended Data Fig. 8f). Thus, the attenuation of LDL transport observed with the loss of SR-B1 from endothelial cells is not related to an alteration of the caveolae microenvironment.

The capacity of other endothelial receptors for LDL to mediate transport of the lipoprotein was also determined[16–18]. Whereas LOX-1 knockdown did not alter nLDL or oxLDL uptake by HAEC (data not shown), RNAi silencing of the LDL receptor (LDLR) or CD36 attenuated uptake, and blocking antibodies had similar effect; however, neither LDLR nor CD36 antibody blockade impacted nLDL or oxLDL transcytosis (Extended Data Fig. 8g–m). Thus, amongst classical lipoprotein receptors, whereas LDLR, CD36 and SR-B1 all promote LDL uptake by human endothelial cells, SR-B1 drives LDL transcytosis.

We next compared the capacity for endothelial LDL transcytosis by SR-B1 and activing receptor-like kinase 1 (ALK1), to which LDL binding and transport has been previously ascribed[19]. LDL transcytosis was decreased to a similar degree by the selective loss of SR-

B1 or ALK1, and there was a further decline with their concurrent knockdown (Extended Data Fig. 9a–f). Thus, both SR-B1 and ALK1 mediate LDL transcytosis in endothelial cells, and they likely do so by different mechanisms. Importantly, endothelial ALK1 expression was normal in SR-B1 ^{EC} mice (Extended Data Fig. 1f), such that the in vivo findings for endothelial SR-B1 and artery LDL delivery, macrophage LDL uptake and atherosclerosis can be attributed specifically to SR-B1.

We then determined if LDL binding to SR-B1 is required for LDL trafficking across endothelium. Endogenous SR-B1 was silenced in HAEC, and expression was reconstituted with wild-type SR-BI or 5 point mutant forms previously (M159E and T165E)[20] or newly identified (F171A, T175A, and E178A) to have attenuated LDL binding (Fig. 2a, Extended Data Fig. 10a–c). Another point mutant, Q445A, with normal LDL binding (Extended Data Fig. 10c) but disrupted SR-B1 interaction with plasma membrane cholesterol[21] was also tested. Whereas reintroduction of wild-type SR-B1 yielded nLDL and oxLDL uptake comparable to that for endogenous SR-B1, cells expressing SR-B1 with decreased LDL binding had markedly diminished LDL uptake; in contrast, cells harboring the Q445A mutant displayed normal LDL uptake (Fig. 2b). The vast majority of LDL transcytosis by SR-B1 was also attenuated if LDL binding was diminished (Fig. 2c). Thus, direct association is essential to LDL trafficking by SR-B1 in endothelial cells.

Since SR-B1 lacks the internalization sequence Tyr-X-X-θ (X is any amino acid and θ is a bulky hydrophobic amino acid) characteristic of other LDL receptors[22], we raised the hypothesis that SR-B1 has an associated partner protein(s) required for its internalization and endothelial LDL transcytosis. As a first test, we generated deletion mutants lacking the C-terminal 15, 23 or 30 residues of SR-B1, designated ΔC15 (Δ495–509), ΔC23 (Δ487–509) and ΔC30 (Δ480–509) (Fig. 2a, Extended Data Fig. 10d–f). Whereas cells expressing ΔC15 had LDL uptake and transcytosis comparable to cells expressing full-length wild-type SR-B1, both processes were attenuated in cells harboring ΔC23 or ΔC30 (Fig. 2d,e). These findings suggested that residues 487–494 (IQAYSESL; Fig. 2a), which are highly conserved in SR-B1 and unique to SR-B1 versus CD36 (Extended Data Fig. 10g), are required. To test this possibility, alanines were substituted for the first four (IQAY) or last four (SESL) residues, or single alanine substitutions were generated (Fig. 2a, Extended Data Fig. 10h–j). Cells expressing the IQAY or SESL mutant or Y490A or S491A displayed dramatically reduced nLDL and oxLDL uptake and transcytosis (Fig. 2f,g); Q488A had attenuated nLDL uptake and transcytosis. Testing various receptor mutants, the findings for binding, uptake and transcytosis were confirmed at nLDL concentrations that saturate LDLR binding (100ug/ml), and endogenous CD36 and LDLR abundance was shown to be unaltered (Extended Data Fig. 10k–n). As such, amino acids 487 to 494 in the C-terminal cytoplasmic tail of SR-B1, IQAYSESL, are critical for LDL uptake and transcytosis by endothelial cells.

Next we tested the hypothesis that residues 487 to 494 of SR-B1 are required for receptor interaction with a cytoplasmic protein(s) necessary for LDL transport. The interactomes of N-terminally-HIS-tagged SR-B1 or SR-B1-ΔC23 in HAEC were evaluated by liquid chromatography/tandem mass spectrometry. One of the 33 proteins demonstrating greater interaction with HIS-SR-B1 versus HIS-SR-B1-ΔC23 was dedicator of cytokinesis 4 (DOCK4), which is a membrane-associated cytoplasmic protein that functions as a guanine

nucleotide exchange factor (GEF) and a participant in actin cytoskeleton regulation[4, 23, 24]. Coimmunoprecipitation experiments in HAEC confirmed DOCK4 interaction with amino acids 487 to 494 of SR-B1 (Fig. 3a–b), and nLDL and oxLDL caused similar 72 to 94% increases in SR-B1-DOCK4 coupling (Fig. 3c). In vivo coexpression of SR-B1 and DOCK4 was demonstrated in aortic endothelium (Fig. 3d), and compared to the atherosclerosis-resistant greater curvature of the aortic arch, both SR-B1 and DOCK4 mRNA levels were increased in the atherosclerosis-prone lesser curvature prior to lesion formation (Fig. 3e–f). Furthermore, in three independent, publicly-available patient cohorts (Fig. 3g–l) both SR-B1 and DOCK4 expression was greater in atherosclerotic arteries versus normal arteries (Fig. 3g–l).

Since DOCK4 mediates PDGF receptor internalization in fibroblasts[24], whether SR-B1 is internalized in endothelial cells, and if so, whether DOCK4 is required was then interrogated in HAEC. Upon the resumption of endocytosis with warming from 4°C to 37°C in the presence of nLDL or oxLDL, the internalization of cell surface biotin-labeled SR-B1 was demonstrable in cells expressing DOCK4, and DOCK4 knockdown attenuated the internalization (Fig. 4a,b). In contrast, transferrin receptor internalization was not affected by DOCK4 deletion, revealing that DOCK4 does not influence endothelial cell SR-B1 endocytosis nonspecifically. It was further found that DOCK4 impacts the degree of LDL binding to SR-B1 but not to LDLR or CD36 (Fig. 4c,d). Importantly, silencing of DOCK4 suppressed SR-B1-dependent LDL uptake and transcytosis assessed using either DiI-labeled or ^{125}I-labeled LDL (Fig. 4e,f, Extended Data Fig. 9g–j), and requirements for both SR-B1 and DOCK4 in LDL transcytosis were confirmed using total internal reflection fluorescence (TIRF) microscopy (Extended Data Fig. 9k–l). In contrast, whereas HDL transcytosis was decreased by SR-B1 silencing as previously shown[13], DOCK4 knockdown had no effect (Fig. 4g), indicating cargo-specific participation of DOCK4 in SR-B1 transport of lipoproteins in endothelial cells. Since DOCK4 is a GEF for Rac1[4], Rac1 participation in LDL trafficking was evaluated. Treatment with LDL caused Rac1 activation, the activation was prevented by silencing either SR-B1 or DOCK4 (Fig. 4h,i), and attenuation of the activation (FExtended Data Fig. 9m) blunted LDL uptake by SR-B1 (Figure 4j). Thus, through a dynamic partnership with DOCK4 serving as a GEF for Rac1, SR-B1 mediates endothelial cell LDL transcytosis to deliver circulating LDL into the subendothelial space to be engulfed by macrophages that become foam cells and promote atherosclerotic lesion formation (Fig. 4k).

It has long been believed that the delivery of circulating LDL into the artery wall that instigates atherosclerosis entails its passive movement through a compromised endothelial barrier at lesion-prone sites, which display higher rates of endothelial senescence and apoptosis, and reduced proliferative reserve and repair capacity[25–27]. We now reveal that active transcellular LDL transport by SR-B1 in the endothelium drives atherogenesis. With mechanistic understanding of disease-promoting artery wall LDL entry now in hand, interventions inhibiting the process may represent a new therapeutic category in the battle against cardiovascular disease.

METHODS

Animal Models

Experiments were performed in male and female wild-type, apoE^{−/−}, LDLR^{−/−}, SR-B1^{fl/fl}, PDZK1^{fl/fl}, VECad-Cre and Alb-Cre mice, or in offspring from their mating. The targeting construct to create floxed SR-B1 mice (SR-B1^{fl/fl}) contained loxP sites inserted in intron 1 and intron 3 of the *Scarb1* gene. The heterozygous SR-B1^{fl/+} mice initially created on mixed background were crossed with apoE^{−/−} and VECad-Cre mice to generate hypercholesterolemic littermates expressing versus deficient in SR-B1 in endothelium (apoE^{−/−};SR-B1^{fl/fl} versus apoE^{−/−};SR-B1^{fl/fl};VECad-Cre designated apoE^{−/−};SR-B1 [EC]), and these were employed in the initial studies of atherosclerosis. The heterozygous SR-B1^{fl/+} mice were also backcrossed to C57BL/6 for more than eight generations, with resulting mice on C57BL/6 background used in experiments that followed. With additional matings LDLR^{−/−};SR-B1^{fl/fl} versus LDLR^{−/−};SR-B1^{fl/fl};VECad-Cre designated LDLR^{−/−};SR-B1 [EC] were also produced. The present use of SR-B1 [EC] for receptor loss-of-function in endothelium contrasts with previous gain-of-function studies performed in mice harboring a Tie2-driven SR-B1 transgene[28]. In that work SR-B1 overexpression yielded atheroprotection. However, the transgene caused a decline in plasma cholesterol and a 50% increase in HDL, and since Tie2-driven gene expression occurs in hematopoietic lineages and endothelium[29], non-endothelial processes cannot be excluded. We also crossed SR-B1 [EC] with Alb-Cre mice (B6.Cg-Tg(Alb-Cre)21Mgn/J, Jackson Laboratory)[30] to generate mice deficient in SR-B1 in hepatocytes, designated SR-B1 [HEP]. The targeting construct to create floxed PDZK1 mice (PDZK1^{fl/fl}), which contained lox P sites inserted in intron 1 and intron 4, was created by BAC recombineering[31]. BAC RP23–405I24 containing the mouse *PDZK1* gene was kindly provided by the Children's Hospital Oakland Research Institute (CHORI). The heterozygous PDZK1^{fl/+} mice initially produced were backcrossed to C57BL/6 for more than eight generations before crossing with apoE^{−/−} and VECad-Cre for studies of endothelial PDZK1 in apoE^{−/−};PDZK1^{fl/fl} versus apoE^{−/−};PDZK1^{fl/fl};VECad-Cre mice, designated apoE^{−/−};PDZK1 [EC]. The cell specificity of SR-B1 or PDZK1 knockdown was evaluated by quantitative RT-PCR or immunoblotting in primary aortic endothelial cells[32] versus myeloid lineage cells purified from bone marrow using anti-CD11b and anti-Gr-1 antibodies (BD Biosciences). Effective excision of the genes in endothelium was also demonstrated by PCR-based genotyping on aortas with versus without intact endothelium. In select experiments LDLR was downregulated in the liver by an IV injection of AAV8-PCSK9 (5×10^{11}gc/mouse). All mice were maintained on standard chow. In studies of atherosclerosis, beginning at weaning at age 4 weeks apoE^{−/−} mice received an atherogenetic diet (D12108C, 20% fat, 1.25% cholesterol, Research Diets Inc.) for 8 weeks, LDLR^{−/−} were fed TD96335 (6.2% fat, 1.25% cholesterol, Harlan Laboratories) for 12 weeks, or following AAV8-PCSK9 injection at 4–5 weeks of age, mice received TD96335 for up to 12 weeks. All animal experiments were approved by the Institutional Animal Care and Use Committee at UT Southwestern.

Atherosclerosis Evaluation and Lipid Analyses

Atherosclerotic lesions were evaluated as previously described[33]. Mice were anesthetized with isoflurane, blood was collected for lipid analyses, and the vascular system was perfused with normal saline administered by left ventricle puncture. Adventitial fat was removed from

the aortic arch prior to in situ imaging. The heart and whole aorta were isolated and placed in 10% formalin for fixation overnight, the heart was dehydrated in 30% sucrose at 4°C overnight and embedded in OCT compound (Fisher Healthcare), and serial frozen sections (8um) of the aortic root were obtained. Ten to fifteen slides with 6 sequential sections each were prepared from each heart, and 1–2 slides per heart were processed for Oil Red O staining of the aortic sinus. For en face analysis, the entire aorta from the aorta root through the bifurcation of the iliac arteries was stained with Oil Red O for 2h at room temperature, adjoining tissues were removed, and the aorta was opened longitudinally and pinned onto a black silicon bed. Lesion quantification was evaluated by morphometry of obtained images using Photoshop software.

Plasma total cholesterol and triglyceride concentrations were determined by colorimetric enzymatic assay (Infinity, Thermo Scientific). HDL levels were determined by precipitating apoB-containing lipoproteins using phosphotungstate-magnesium and measurement using the HDL Cholesterol Kit (Wako)[34]. Plasma lipid profiles were obtained by column fractionation and measurements of fraction cholesterol content[35].

Cardiac Phenotyping

Using previously-described methods[8], hearts were excised and rinsed in PBS and fixed in 10% formalin for 48h, embedded in paraffin, and sectioned at 5um intervals. Hematoxylin and eosin staining and Masson's trichrome staining were performed following standard procedures. Macrophage content was evaluated by immunohistochemistry using anti-CD68 antibody (ab955, Abcam). Survival curves were generated to compare the overall outcome of SR-B1$^{fl/fl}$ controls and SR-B1 ^{HEP} that were made hypercholesterolemic with AAV8-PCSK9.

In Vivo Leukocyte-endothelial Adhesion and Endothelial Permeability

Leukocyte-endothelial adhesion was assessed using our previously-established method[35]. Briefly, in 4- to 5-week-old male mice, endogenous leukocytes were fluorescence labeled by injection with 100ul Rhodamine-6G (0.05% w/v) via optic vascular plexus. Under anesthesia the mesentery was exposed on a clear dish for the observation and recording of images of leukocyte adhesion and rolling in the mesenteric microvasculature using a Regita digital camera (400x magnification; QImaging). The velocity of leukocyte rolling was calculated using Image-Pro V.6.2 (Media Cybernetics). To evaluate adhesion under both control and pro-inflammatory conditions, mice received an IP injection of normal saline or TNFα (0.3ug/mouse) 4h prior to study.

To evaluate endothelial permeability, mice were injected retro-orbitally with 0.5% (w/v) Evans blue dye dissolved in normal saline (4ul/g body weight) as described previously[36]. After 1h, the mice were euthanized and perfused via the left ventricle with 10ml cold PBS. The entire aorta was isolated, washed in PBS, and placed in formamide at 55°C for 48h. Following centrifugation the dye concentration was determined by measuring absorbance at 650nm with comparison to a standard curve.

In Vivo Aorta LDL Uptake

Human native LDL (nLDL) was kindly provided by Drs. J. Goldstein and M. Brown (UT Southwestern). Briefly, LDL particles were isolated by ultracentrifugation from normal human plasma and stored in buffer containing 0.27mM EDTA at 4°C. To generate oxidized LDL (oxLDL), nLDL particles at a concentration of 1 mg protein/ml were incubated with 5uM $CuSO_4$ at 37°C for 24h, 100uM EDTA and 20uM butylated hydroxytoluene were added to terminate oxidation, and the resulting samples were dialyzed with PBS for 48h. Murine LDL (density 1.019–1.063 g/ml) and VLDL/IDL (density 1.006–1.019 g/ml) was obtained from pooled LDLR$^{-/-}$ mouse plasma by sequential ultracentrigation[37]. To optimize their detection, nLDL, oxLDL or murine LDL or VLDL/IDL were labeled with 1,1'dioctadecyl-3,3,3',3'-tetramethylindocarbocyanine perchlorate (Dil, Invitrogen) at 37°C for 16h, centrifuged at $16,000 \times$ g for 10min at 4°C, and dialyzed with PBS for 24h. Dil-labeled LDLs were stored at 4°C and used within 1–2 weeks[38].

To evaluate aorta LDL uptake in vivo, following receipt of an atherogenic diet for one week, 8–10 week-old mice were injected retro-orbitally with 100ug Dil-LDL, and 0 to 4h later the mice were anesthetized and perfused with ice-cold PBS for 5min, and the thoracic aorta was isolated. Following removal of the adventitia, the aorta was digested in RIPA buffer (Thermo Fisher) containing protease inhibitor cocktail (P8340, Sigma), and DiI-labeled lipoprotein content was quantified either using a fluorometer (POLARstar Omega, BMG LABTECH) and measurement of aorta homogenate protein content (Pierce BCA Protein Assay Kit), or when human LDL was employed, by immunoblotting with anti-human apoB antibody (MA5–15851, ThermoFisher) and anti-calnexin antibody (ADI-SPA-860-F, Enzo Life Sciences) to assess protein loading. To test the impact of a pharmacologic intervention targeting SR-B1, in select experiments the mice received either control sera or SR-B1 blocking antibody (1:2 dilution, 200ul)[39] both16h and 1h prior to the administration of DiI-LDL.

To visualize LDL transport across the endothelial monolayer in vivo, 4h following intravenous DiI-LDL administration the aorta was isolated, subjected to Hoechst staining (5ug/ml) at 4°C for 30min to identify nuclei, washed X3, and then fluorescence confocal microscopy was performed on the luminal surface using a 20X objective and a Zeiss LSM710 NLO two-photon excitation microscope. The methods were adapted from approaches employed to image the brain vasculature of mice[40]. A minimum of three randomly-selected regions in the ascending aorta were imaged per mouse to a depth of approximately 50μm (Z=1–2μm), and the data obtained were analyzed by Zeiss ZEN software.

To quantify LDL uptake by arterial wall macrophages/foam cells, 4h following intravenous DiI-LDL administration, CD45$^+$, F4/80$^+$ cells were isolated from the aorta using our established approach[41]. The aorta was digested with liberase TH (4 U/ml, Roche), deoxyribonuclease (DNase) I (0.1 mg/ml, Sigma), and hyaluronidase (60 U/ml, Sigma) at 37°C for 2h, and flow cytometry (BD Biosciences LSR II) was performed with 1:200 dilutions of anti-CD45 (clone 30-F11) and anti-F4/80 (clone BM8) antibodies obtained from Biolegend as well as detection of Di-I signal. Data obtained were analyzed using FlowJo software (Treestar).

Electron Microscopy

The subcellular localization of intravascularly-administered LDL particles and SR-B1 in aortic endothelial cells was evaluated by electron microscopy (EM). Following fasting for 4h, 10 week-old C57BL/6 mice were anesthetized and the aorta was cleared of blood in situ by perfusion with PBS with 0.25% glucose at 37°C. The thoracic aorta was then perfused (15ml/min) with colloidal gold-labeled nLDL (10–15nm diameter, 50ug/ml in EBM2 medium plus 1%BSA, 37°C)[42, 43] from proximal to distal, and the perfusate was recirculated. Ten minutes later the thoracic aorta was washed with ice-cold PBS (10 ml) to remove unbound LDL, harvested and opened longitudinally, and incubated in EM fixation solution (4% PFA in 0.1M phosphate buffer pH7.4, containing 0.1% glutaraldehyde) for 30min at room temperature. SR-B1 was visualized using a primary antibody to mouse SR-B1 (Novus, NB400–104)[44] and a fluoronanogold (1.4nm diameter)-conjugated secondary antibody (Alexa Fluor 488-FluoroNanogold Fab' goat anti-rabbit IgG, 7204, Nanoprobes). The immunogold-labeled samples were further gold-enhanced for 2.5 min using a gold enhancement kit (Nanoprobes). After washing with water and 0.1M cacodylate buffer, samples were fixed with 1% OsO_4 and 0.8% potassium ferricyanide in 0.1M cacodylate buffer for 1h, stained en bloc with 2% aquaous uranyl acetate, dehydrated with increasing concentration of ethanol, and embedded in Epon. Blocks were sectioned with a diamond knife (Diatome) on a Leica Ultracut 7 ultramicrotome (Leica Microsystems) and collected onto copper grids. Images were acquired on a JOEL 1400 Plus transmission electron microscope equipped with a LaB6 source using a voltage of 120 kV, and the images were captured by an AMT BIOSPRINT 16M-ActiveVu mid mound CCD camera. In sections processed in the absence of primary anti-SR-B1 antibody, the gold particles detecting SR-B1 were absent.

Cultured Cell Models, Gene Silencing and Reconstitution

Primary human aortic endothelial cells (HAEC) obtained from Lonza were maintained in EBM2 medium with 10% (v/v) fetal bovine serum and studied at passage 3 to 6. Gene silencing was accomplished using predesigned and validated siRNAs targeting SR-B1 (s2648), PDZK1 (s10282), LOX1 (s9842), LDLR (S224006), or CD36 (s534752) (Life Technologies Corp.), and effective knockdown was confirmed by immunoblot analysis. ALK1 was silenced using shRNA (TRCN0000000354) (Sigma), and successful loss of ALK1 was confirmed by quantitative RT-PCR and measurement of SMAD1/5 Ser463/465 phosphorylation in response to BMP9 treatment (10ng/ml) for 0 to 120 min[19]. In studies of DOCK4, gene silencing was done with a lentiviral shuttle plasmid for shRNA targeting human *DOCK4* (TRCN0000288692) (Sigma). In select studies including the experiments determining the SR-B1 structural features required for LDL transport, the endogenous receptor was knocked down by shRNA targeting the 3'UTR of the human *SR-B1* gene (5'-CCGGGCTCGTCAACAAGCACTGTTCCTCGAGGAACAGTGCTTGTTGACGAGCTTTTTG-3' in pLKO.1-TRC). Wild-type or mutant forms of SR-B1 were reintroduced using CMV promoter-driven lentiviral constructs. Polybrene (8ug/ml, EMD Millipore) was added to the medium to enhance lentiviral transduction efficiency, and experiments were performed 48h later. The SR-B1 mutants were generated using cDNA encoding human *Scarb1* (NM_005505, Sino Biological Inc.) and the Virapower Lentiviral Expression System (ThermoFisher). Shuttle plasmid (5ug), psPAX2 packaging plasmid (3ug), and pMD2.G

envelope plasmid (2ug) were co-transfected into HEK-293FT cells in DMEM using Fugene6. Six hours and 48h post-transfection, the medium was replaced with DMEM containing 2mM caffeine and 30% FBS. The lentiviral particles were harvested 48h and 72h after transfection, passed through a 0.45um filter (Millipore) to remove cellular debris, concentrated by ultracentrifugation at 100,000 × g for 90min at 4°C, and resuspended in Dubelcco's phosphate-buffered saline (Gibco) overnight at 4°C. The lentiviral preparations were then aliquotted and stored at −80°C, and SR-B1 mutations were confirmed by sequencing.

Total cell abundance of the reconstituted wild-type or mutant forms of SR-B1 was evaluated by immunoblot analysis 48h following lentiviral transduction. To assess their cell surface abundance, cells were incubated with anti-SR-B1 antibody directed against the extracellular domain (NB400–134, Novus Biologicals) on ice for 30min, washed X3, incubated with alexa488-conjugated secondary antibody for 30min at 4°C, washed X3, and subjected to flow cytometry (BD Biosciences LSR II).

Quantitative RT-PCR

Transcript abundance was evaluated in mouse aorta, mouse aortic endothelial cells or human endothelial cells by quantitative RT-PCR using previously established methods[35].

LDL Binding, Uptake and Transcytosis

To evaluate DiI-LDL binding, cells in 24-well plates were precooled at 4°C for 10min, incubated with 50 ug/ml DiI-LDL at 4°C for 10 min, washed X3 with ice-cold PBS and lysed in 1% Triton X100 at room temperature for 10min with shaking, and fluorescence was quantified using a fluorometer (POLARstar Omega, BMG LABTECH) and normalized to total protein content.

LDL uptake studies entailed cell incubation with 10ug/ml DiI-LDL for 4h at 37°C. In select experiments the DiI-LDL incubation followed a 1h preincubation with DMSO control vehicle versus the SR-B1 inhibitor BLT-1 (10uM, Sigma)[45], or control unrelated IgG versus anti-SR-B1 blocking antibody. DMSO control had no effect on LDL transport. Cells were washed with PBS and lysed for the measurement of fluorescence intensity by fluorometer. For imaging of LDL uptake, experiments were performed with cells seeded onto glass coverslips precoated with collagen I. Following DiI-LDL incubations the cells were fixed with 1% formalin in PBS for 10min at room temperature, nuclei were stained with DAPI, mounting media was added (Vector Laboratories, Inc.), and fluorescence microscopy was performed at 40X magnification with a Nikon Eclipse TE2000-E microscope.

LDL transcytosis was studied using approaches derived from previously-reported methods[32]. Cells were seeded twice, 24h apart, onto 0.4um pore PET Transwell inserts (3610, Corning, Inc.) coated with collagen I (BD Bioscience), with or without lentiviral transduction overnight. Transcytosis was evaluated 48h later, at which time measurements of transepithelial electrical resistance using an epithelial volt-ohmmeter (World Precision Instruments) confirmed the establishment of a confluent monolayer. FITC-dextran (M.W. 3000; Invitrogen) was used to assess paracellular transport. Cells were incubated simultaneously for 2h with FITC-dextran and 50ug/ml DiI-LDL added to the upper chamber,

and the fluorescence intensity of FITC and DiI in the lower chamber was measured using a fluorometer (POLARstar Omega, BMG LABTECH). FITC-dextran transport was 2 to 3% and similar for control cells and cells in which SR-B1 expression was reconstituted. Infrequently-observed inserts displaying paracellular transport more than 5% were discarded. The addition of 50-fold excess LDL decreased the DiI signal for transcytosis by 75%. In select experiments interventions were placed in the upper chamber for 1h prior to the addition of DiI-LDL. Under control conditions the percent transcytosis of DiI-LDL was approximately 12%, and the data shown are normalized to control values. HDL transcytosis was also performed using DiI-labeled lipoprotein. The validity of the uptake and transcytosis assays employing DiI-LDL was confirmed using nLDL labeled with iodine-125 by the Bolton-Hunter method. In uptake studies, cells were incubated with 10ug/ml ^{125}I-LDL for 4h, washed with PBS and lysed with 0.1N NaOH, and radioactivity was quantified in the cell lysate using a Wizard Automatic Gamma Counter (PerkinElmer) and expressed relative to protein content. For transcytosis studies, cells were incubated with 50ug/ml ^{125}I-LDL for 2h and radioactivity in both the upper and lower chambers was quantified.

To provide an additional means to confirm the findings obtained for transcytosis, total internal reflection fluorescence (TIRF) microscopy was employed[10, 19]. Time-lapse imaging of transcytosis was carried out on an OMX SR microscope in Ring TIRF mode (GE Healthcare Life Science). Briefly, endothelial cells seeded in 35 mm glass bottom dishes (MatTek, MA) were treated with 50μg/ml DiI-nLDL in EGM2 medium with HEPES at 4°C for 10 min to allow the LDL to bind to the apical cell surface without internalization. Endothelial cells pretreated with Dyngo4A (30μM; Abcam) for 30 min were processed in parallel to confirm dynamin dependence of transcytotic events[10]. The cells were rinsed with cold PBS, and warm medium was added, and the dish was placed in a 37°C live cell incubation chamber on the microscope stage for 2 min before imaging. An Olympus ApoN 60× 1.49 NA lens was used for through the objective TIRF with 561 nm laser excitation. The TIRF angle was set at 96% of the back aperture of the lens, for an estimated nominal penetration depth of 70 nm. Images were acquired using a cooled sCMOS camera with a 50 ms exposure at 150 ms intervals for a minimum of 40 sec. At least 15 randomly-selected cells were imaged for each condition, and the transcytosis events in the first 5 to 6 cells imaged were quantified using Imaris 9.2.0. image analysis software (Bitplane, Zurich Switzerland). The Spots Wizard was used to identify DiI-labeled LDL particles and track them over time. The spots were filtered based on mean squared displacement over time to exclude those exhibiting Brownian motion or active transport, and statistics measured by Imaris were exported for analysis in Excel. Numbers of transcytosis events captured in 200 frames were determined using criteria reported previously[19].

NOS Assays

To assess caveolae function in cultured endothelial cells, the conversion of ^{14}C-L-arginine to ^{14}C-L-citrulline was measured in intact cells under basal conditions or with the addition of VEGF (100ng/ml) or HDL (20ug/ml)[46]. In select studies caveolae were disrupted by cell treatment with methyl-β-cyclodextrin (10mM for 60min) prior to the evaluation of NOS activation.

Liquid Chromatography/Tandem Mass Spectrometry (LC/MS-MS)

To identify proteins that interact with SR-B1 in endothelial cells, SR-B1 immunoprecipitation was facilitated by N-terminal HIS tagging of the receptor. N-terminal tagging was chosen because the SR-B1 N-terminal tail does not participate in any known function of the receptor[47], and the addition of the N-terminal HIS tag did not affect LDL uptake by SR-B1 in HAEC (data not shown). An N-terminal HIS tag was also placed on the SR-B1- C23 truncated form of the receptor. Endogenous SR-B1 was silenced in HAEC, receptor expression was reconstituted with either HIS-SR-B1 or HIS-SR-B1- C23, SR-B1 was immunoprecipitated with anti-HIS antibody, and the associated proteins were evaluated by liquid chromatography/tandem mass spectrometry (LC/MS-MS). Immunoprecipitated protein samples were electroporated 10mm into the top of a pre-cast SDS-PAGE gel (Bio-Rad), stained with Coomassie blue and excised. Following alkylation and reduction with dithiothreitol and iodoacetamide (Sigma), samples were digested overnight with trypsin (Promega) and then subjected to LC/MS-MS using a QExactive mass spectrometer (Thermo Electron) coupled to an Ultimate 3000 RSLC-Nano liquid chromatography system (Dionex). Peptides were loaded onto a 180μm i.d., 5cm long, self-packed column containing 1.9μm C18 resin (Dr. Maisch, Ammerbuch, Germany) and eluted with a gradient of 0–40% buffer containing 80% (vol/vol) ACN, 10% (vol/vol) trifluoroethanol, and 0.08% formic acid for 60 min. Up to 10 high-energy, collision-induced dissociation fragment spectra were obtained for each full spectrum acquired. Raw MS data files were converted to peak list format using ProteoWizard Msconvert, and the resulting files were analyzed using the Central Proteomics Facilities Pipeline[48]. Label-free quantitation of proteins across samples was performed using the Normalized Spectral Index method (SINQ)[49].

Co-immunoprecipitation and Immunoblot Analyses

Co-immunoprecipitation studies were performed to evaluate proteins interacting with either HIS-tagged wild-type or mutant SR-B1, or DOCK4 in HAEC. Cells were incubated with lysis buffer containing 25mM Tris-HCl, pH7.4, 150mM NaCl, 1% NP-40, 1mM EDTA, and 5% glycerol (Thermo Fisher) supplemented with protease inhibitor cocktail (P8340, Sigma) on ice for 1h with vortexing every 20min. Supernatants collected following centrifugation at $14,000 \times g$ at 4°C for 10 min were incubated with control IgG, anti-DOCK4 (ab85723, Abcam) or anti-HIS tag (ab18184, Abcam) antibody at 4°C overnight, and protein A/G plus agarose beads (Pierce) were added for 2h. The beads were pelleted by centrifugation, washed X3, and the bound proteins were eluted with SDS sample buffer and analyzed by SDS-PAGE and immunoblotting. Primary antibodies employed were anti-DOCK4 antibody, and anti-SR-B1 antibody recognizing the N-terminus (ab52629, Abcam) to identify C-terminally-truncated SR-B1. HRP-conjugated secondary antibodies and chemiluminescent detection and densitometry were then employed.

In cell culture experiments additional immunoblot analyses were performed employing anti-SR-B1 (NB400–113 and NB400–134,Novus; ab52629, Abcam), anti- PDZK1 (ab64856, Abcam), anti-LOX-1(MAB1798, R&D Systems), anti-LDLR (AF2148, R&D Systems), anti-CD36 (NB400–144,Novus; MA-5–14112, Invitrogen) and anti-transferrin receptor (ab84036, Abcam) antibodies. Protein loading was assessed using anti-GAPDH (sc-365062, Santa Cruz) antibody.

Gene Expression Profiling in Human Atherosclerotic versus Normal Arteries

To compare SR-B1 and DOCK4 in human atherosclerotic versus normal arteries, three publicly available independent human atherosclerosis cohorts with gene expression data were downloaded from Gene Expression Omnibus (GEO, https://www.ncbi.nlm.nih.gov/geo/). The accession numbers were GSE116243, GSE40231, and GSE43292. For the GSE116243 cohort (Cohort I), which included atherosclerotic aortic lesions, the gene expression profiling was generated by RNA sequencing through Illumina HiSeq 2500. For comparison, RNA sequencing datasets of aorta from healthy donors were downloaded from Genotype-Tissue Expression (GTEx) database with accession number phs000424.v6.p1. RNA-seq reads from FASTQ files were quality-filtered using FASTQ Quality Filter (-q 20 – p 75) from FASTX-toolkit (http://hannonlab.cshl.edu/fastx_toolkit/). The filtered reads were then aligned to hg38 reference genome by HISAT2 aligner[50]. Cufflinks[51] was used to assemble and estimate the relative abundances of transcripts at the gene and transcript level. For the GSE40231 cohort (Cohort II), which compared atherosclerotic aortic lesions with internal mammary artery from the same subjects, gene expression profiling was generated by Affymetrix Human Genome U133 Plus 2.0 Array. Signal intensity CEL files were downloaded from GEO and then processed by Affymetrix Power Tools (APT) with Robust Multiarray Average (RMA) method. For the GSE43292 cohort (Cohort III), which matched atherosclerotic carotid artery with healthy carotid artery from the same subject, gene expression profiling was generated by Affymetrix Human Gene 1.0 ST Array. CELL files were downloaded from GEO and then were analyzed using R/BioConductor package with RMA method and custom PERL scripts. Data are presented as box-and-whisker plots, with the central lines denoting medians, edges of the box representing upper and lower quartiles, and whiskers showing minimum and maximum values after excluding outliers outside 1.5 times the interquartile range. Notably although the analyses of the three cohorts utilized distinct technology platforms to measure gene expression, the same findings were obtained.

SR-B1 Internalization

To evaluate SR-B1 internalization, following surface protein labeling with 2mM Sulfo-NHS-SS-biotin at 4°C for 30min[33], the cells were washed with 100mM glycine in PBS to quench non-reacted biotinylation reagent, and then incubated with 50 ug/ml Dil-LDL at 37°C for 0 to 10min. Remaining cell surface biotin was cleaved with 50mM reduced glutathione (Sigma), cells were lysed in RIPA buffer, biotinylated proteins were isolated by incubating with streptavidin magnetic beads overnight at 4°C, the bound proteins were eluted with loading buffer, and immunoblot analysis was performed. To assess the efficacy of SR-B1 biotinylation, whole cell lysates were obtained at 0 to 10min of incubation, and total biotinylated SR-B1 was quantified by immunoblotting. To evaluate the internalization of another cell surface protein, the abundance of internalized transferrin receptor and total biotinylated transferrin receptor was determined in a parallel manner.

### Rac1 Activity Assay and Rac1 Loss-of-function

Rac1 activity was evaluated by affinity purification and immunoblotting (Millipore). Following cell treatment, cell lysates were incubated with PAK1 PBD agarose to bind activated, GTP-bound Rac1, and its abundance was determined by immunoblotting. Total

Rac1 in cell lysates was also evaluated by immunoblotting. To determine the role of Rac1 in endothelial cell LDL uptake, cells were transduced with adenovirus encoding GFP or a dominant-negative form of Rac1 (T17N)[52] with MOI 100 for 48h prior to the uptake assay. The impact of pharmacologic inhibition was also tested, pretreating cells with vehicle or the Rac1 inhibitor NSC23766 (100uM)[53] for 1h prior to the uptake assay.

Statistics and Reproducibility

Results are expressed as mean±SEM. Comparisons between two groups were done by two-sided Student's t test unless otherwise noted, and analysis of variance (ANOVA) with Dunnett's post-hoc testing was performed to compare 3 or more groups. A p value <0.05 was considered statistically significant. When representative findings are presented, similar results were obtained at least three times. Observations in cell culture were confirmed in three independent experiments.

Extended Data
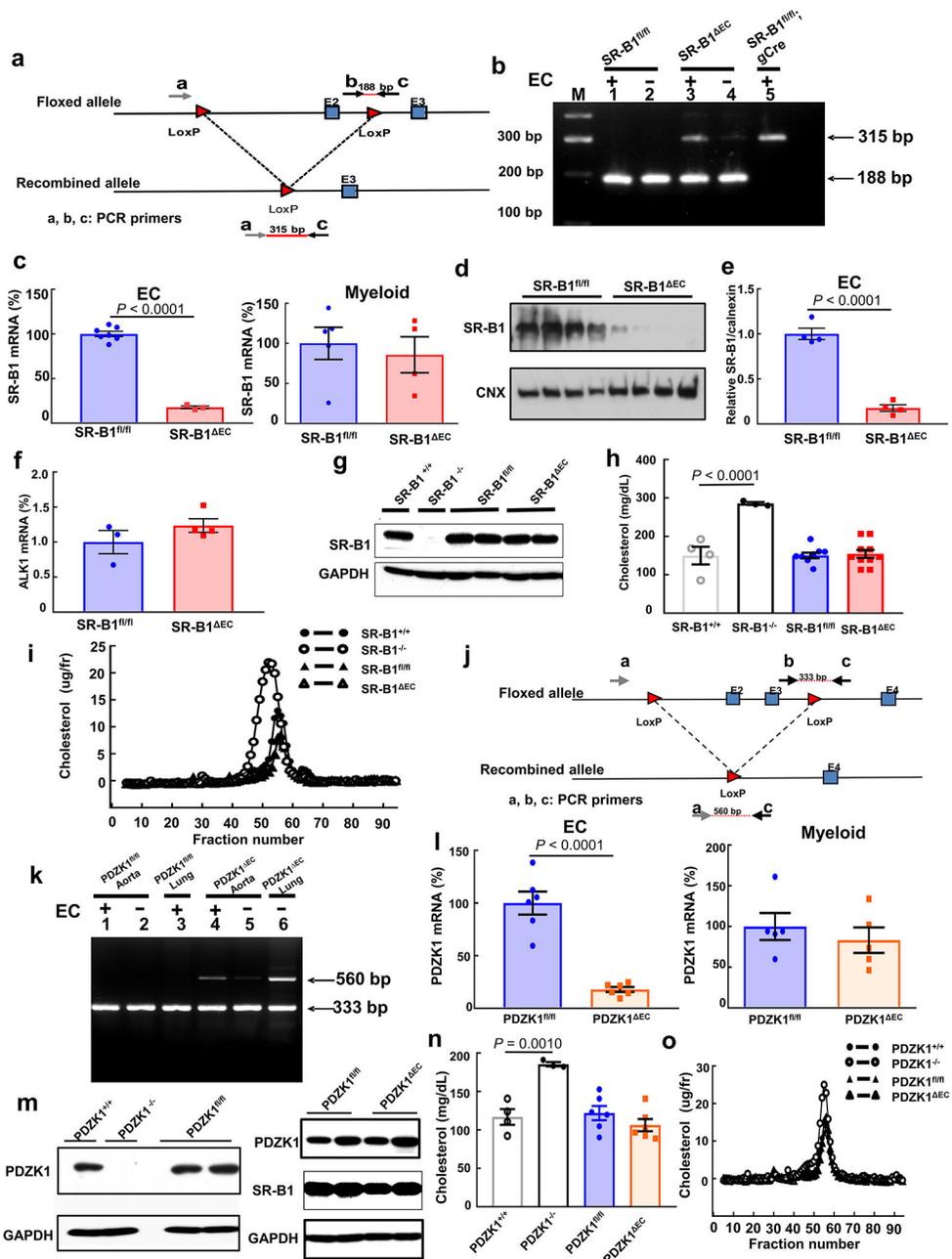
**Extended Data Figure 1. Establishment of mice lacking endothelial SR-B1 or PDZK1.**

a,j, Schematics of the gene-targeting strategies to generate floxed alleles of *Scarb1* (**a**) and *PDZK1* (**j**) to create SR-B1^{fl/fl} and PDZK1^{fl/fl} mice. In SR-B1[fl], exon 2 was floxed, and in PDZK1[fl], exons 2 and 3 were floxed. The recombined alleles following Cre recombinase introduction are also shown. **b,k**, Using primers depicted in **a** and **j**, PCR-based genotyping was performed on aortas with versus without intact endothelial cells (EC). Aortas were obtained from floxed mice, and mice with *Scarb1* or *PDZK1* deleted selectively from EC (SR-B1 [ΔEC] or PDZK1 [ΔEC]). In genotyping evaluating *Scarb1* excision (**b**), additional samples were obtained from SR-B1^{fl/fl} mice expressing Cre recombinase globally (gCre). In

genotyping evaluating PDZK1 excision (**k**), lung samples were also studied. **c,l**, Quantitative real-time PCR analysis of SR-B1 (**c**) or PDZK1 expression (**l**) in primary aortic EC (n=6) and bone marrow-derived myeloid lineage cells (n=5). **d,e,f**, SR-B1 protein abundance (**d,e**, n=4) and ALK1 transcript levels (**f**, n=4) were evaluated in aortic endothelial cells from SR-B1$^{fl/fl}$ and SR-B1^{EC} mice; summary data for SR-B1 protein are in **e**. The uncropped versions of all immunoblots shown are provided in Supplementary Figure 1. **g,m**, Immunoblotting of SR-B1 (**g**) or PDZK1 protein (**m**) abundance in liver. **h,n**, Plasma cholesterol levels. For SR-B1 studies, n=4,3,9 and 10 mice, respectively, for PDZK1 studies, n=4, 3, 6 and 6 mice, respectively. **i,o**, Representative lipoprotein profiles. Data are mean ±SEM; in c, e, and I, P values by two-sided Student's t test are shown, and in h and n, P values by ANOVA with Dunnett's post hoc testing are shown.
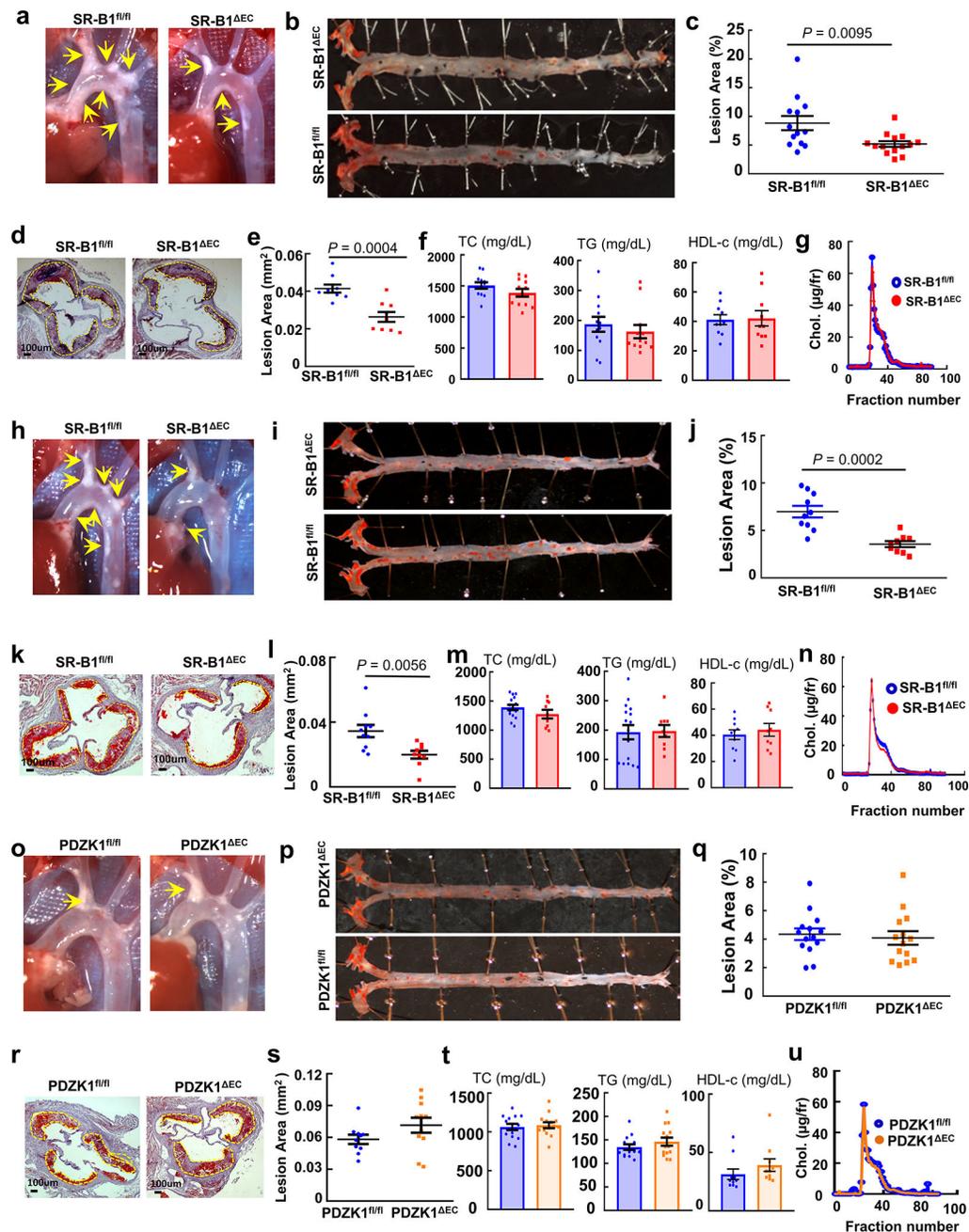
Extended Data Figure 2. Atherosclerosis is promoted by endothelial SR-B1 but not by endothelial PDZK1, and neither endothelial SR-B1 nor PDZK1 affect circulating lipids. Findings are shown for SR-B1 in mixed background females (**a-g**) and in C57BL/6 males (**h-n**), and for PDZK1 in C57BL6 males (**o-u**). Representative in situ aortic arch images of atherosclerotic plaque (yellow arrows) are in **a, h** and **o**, representative images for lipid-stained lesions in *en face* aortas are in **b, i** and **p**, and representative images for lipid/hematoxylin-stained aortic root sections (lesions outlined by yellow dashed line, magnification 40X) are in **d, k** and **r**. Lesion area quantitation in *en face* aortas (percent total surface area) are in **c** (n=13 and 14, respectively), **j** (n=10 and 9, respectively) and **q** (n=14/

group), and quantitation in aortic root sections are in **e** (n=9/group), **l** (n= 10 and 9, respectively) and **s** (n=10 and 11, respectively). Plasma total cholesterol (TC), triglyceride (TG), and HDL cholesterol (HDL-c) are in **f** (n=12/group for TC and TG, and 10/group for HDL-c), **m** (n=16 and 9, respectively for TC and TG, and n=10 and 9, respectively for HDL-c), and **t** (n=14/group for TC and TG, and 10/group for HDL-c); findings for SR-B1$^{fl/fl}$, SR-B1^{EC} and PDZK1^{EC} are shown in blue, red and orange, respectively. Representative lipoprotein profiles are in g, n and u. Data are mean±SEM. In c, e, j and l, P values by two-sided Student's t test are shown.
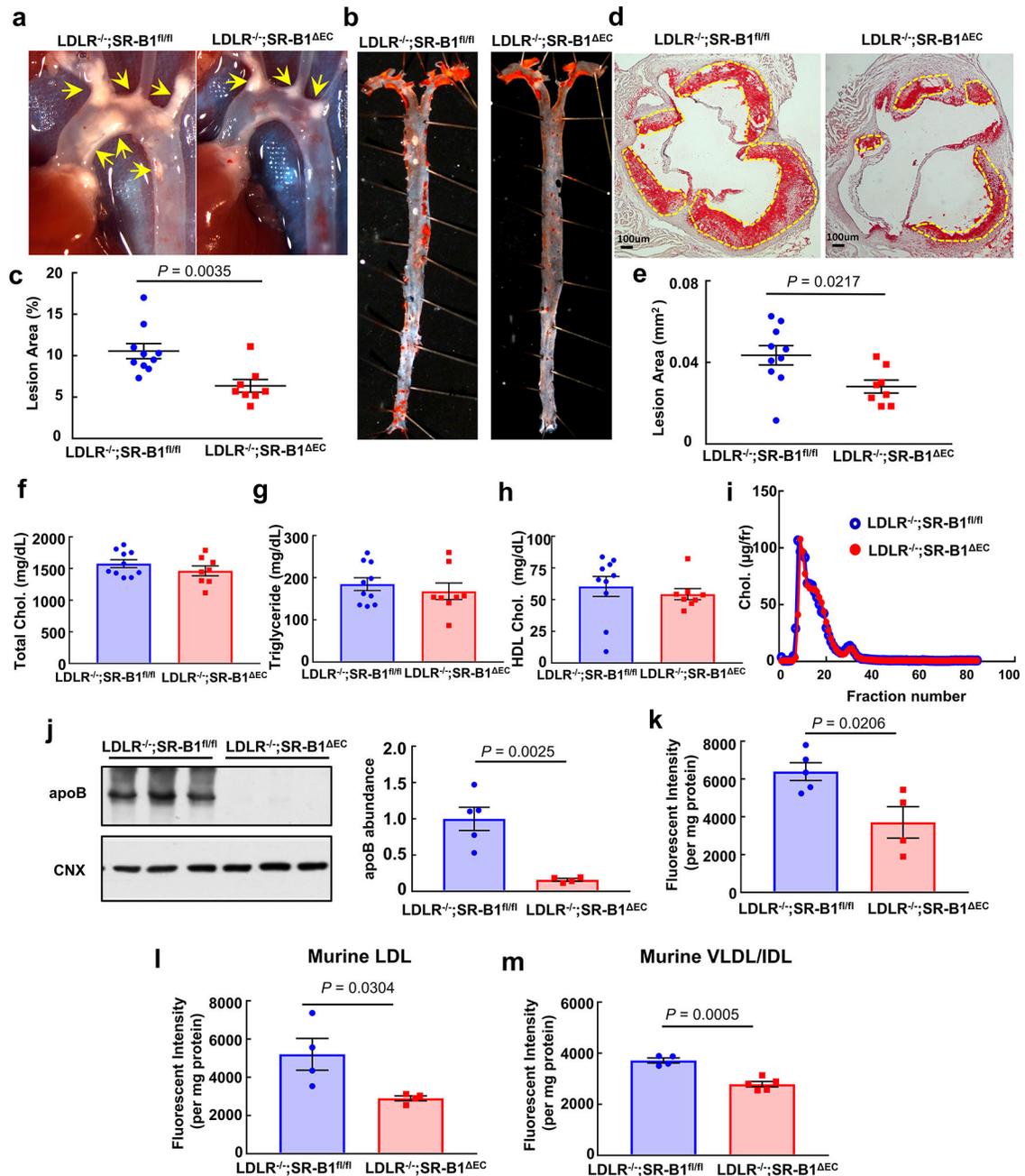
Extended Data Figure 3. Endothelial SR-B1 promotes atherosclerosis in LDLR null mice by driving LDL entry into the artery wall.

a, Representative in situ aortic arch images of atherosclerotic plaque (yellow arrows) in male LDLR$^{-/-}$;SR-B1$^{fl/fl}$ and LDLR$^{-/-}$;SR-B1$^{\Delta EC}$ mice. **b**, Representative lipid-stained *en face* images of aortas. **c**) Quantitation of lesion areas in *en face* aortas (percent of total surface area); n=10 and 8, respectively. **d**, Representative lipid/hematoxylin-stained aortic root sections (lesions outlined by yellow dashed line, magnification 40X). **e**, Quantitation of lesion areas in aortic root sections; n=10 and 8, respectively. **f-h**, Plasma total cholesterol (**f**), triglyceride (**g**), and HDL cholesterol (**h**), n=10 and 8, respectively. **i**, Representative

lipoprotein profiles. **j,k**, Aorta dil-nLDL uptake. Human apolipoprotein B abundance (**j**) or Dil fluorescence intensity (**k**) was evaluated in aorta homogenates 4h following IV DiI-nLDL injection. Left panel in j displays a representative immunoblot with 3 samples per group, and in j and k, n= 5/group. **l,m**, Aorta dil-labeled mouse LDL (**l**) or mouse VLDL/IDL (**m**) uptake in LDLR$^{-/-}$;SR-B1$^{fl/fl}$ and LDLR$^{-/-}$;SR-B1 ^{EC} mice (n=4 and 5, respectively). Data are mean±SEM, P values by two-sided Student's t test are shown.
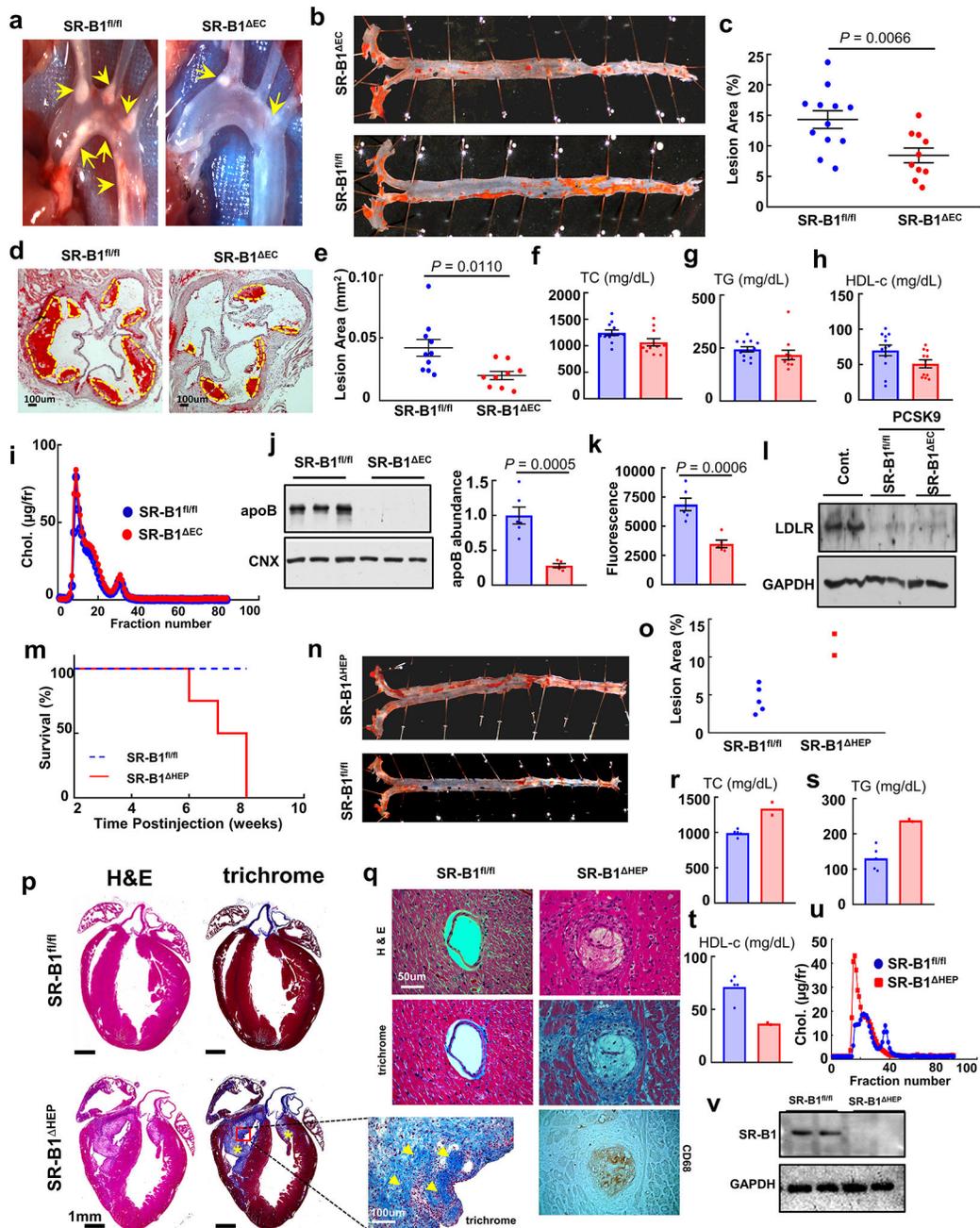
Extended Data Figure 4. Endothelial SR-B1 and hepatocyte SR-B1 have opposing impact on atherosclerosis.
Using AAV8-PCSK9, hypercholesterolemia was induced in male SR-B1^{fl/fl} mice, and in SR-B1[ΔEC] or SR-B1[ΔHEP] mice lacking SR-B1 selectively in endothelial cells or hepatocytes, respectively. Findings in SR-B1^{fl/fl} versus SR-B1[ΔEC] are in **a-l**, and findings in SR-B1^{fl/fl} versus SR-B1[ΔHEP] are in **m-v**. **a**, Representative in situ aortic arch images of atherosclerotic plaque (yellow arrows) in SR-B1^{fl/fl} and SR-B1[ΔEC] mice. **b**, Representative lipid-stained *en face* images of aortas. **c**) Quantitation of lesion areas in *en face* aortas (percent of total surface area); n=12 and 10, respectively. **d**, Representative lipid/hematoxylin-stained aortic

root sections (lesions outlined by yellow dashed line, magnification 40X). **e**, Quantitation of lesion areas in aortic root sections; n=10 and 9, respectively. **f-h**, Plasma total cholesterol (**f**), triglyceride (**g**), and HDL cholesterol (**h**), n=12 and 11, respectively. **i**, Representative lipoprotein profiles. **j,k**, Aorta dil-nLDL uptake. Human apolipoprotein B abundance (**j**) or Dil fluorescence intensity (**k**) was evaluated in aorta homogenates 4h following IV injection (n=6 and 5, respectively). Left panel in j displays a representative immunoblot with 3 samples per group. **l**, LDLR abundance in livers of control mice and SR-B1$^{fl/fl}$ and SR-B1 ^{EC} mice administered AAV-PCSK9. Immunoblot depicts protein abundance for 2 samples per group. **m**, Survival curves for SR-B1$^{fl/fl}$ and SR-B1 ^{HEP} mice, n=5 and 4, respectively. **n**, Representative lipid-stained *en face* images of aortas. **o**, Quantitation of lesion areas in *en face* aortas. Aortas and plasma were only available from two SR-B1 ^{HEP} mice. **p**, Longitudinal sections of SR-B1$^{fl/fl}$ and SR-B1 ^{HEP} hearts stained with H&E or trichrome (healthy myocardium, red/brown; fibrotic tissue, blue; yellow asterisks and arrows indicate areas of severe fibrosis). Images shown mirror those obtained in all 3 hearts per group that underwent histological analysis. **q**. Coronary arteries of SR-B1$^{fl/fl}$ and SR-B1 ^{HEP} mice stained with H&E or trichrome, and coronary artery of SR-B1 ^{HEP} mouse stained with anti-CD68 to detect macrophages. **r-t**, Plasma total cholesterol (TC), triglyceride (TG), and HDL cholesterol (HCL-c). **u**, Representative lipoprotein profiles. **v**, Immunoblotting of SR-B1 abundance in liver, showing findings for 2 samples per group. Data are mean±SEM, P values by two-sided Student's t test are shown.
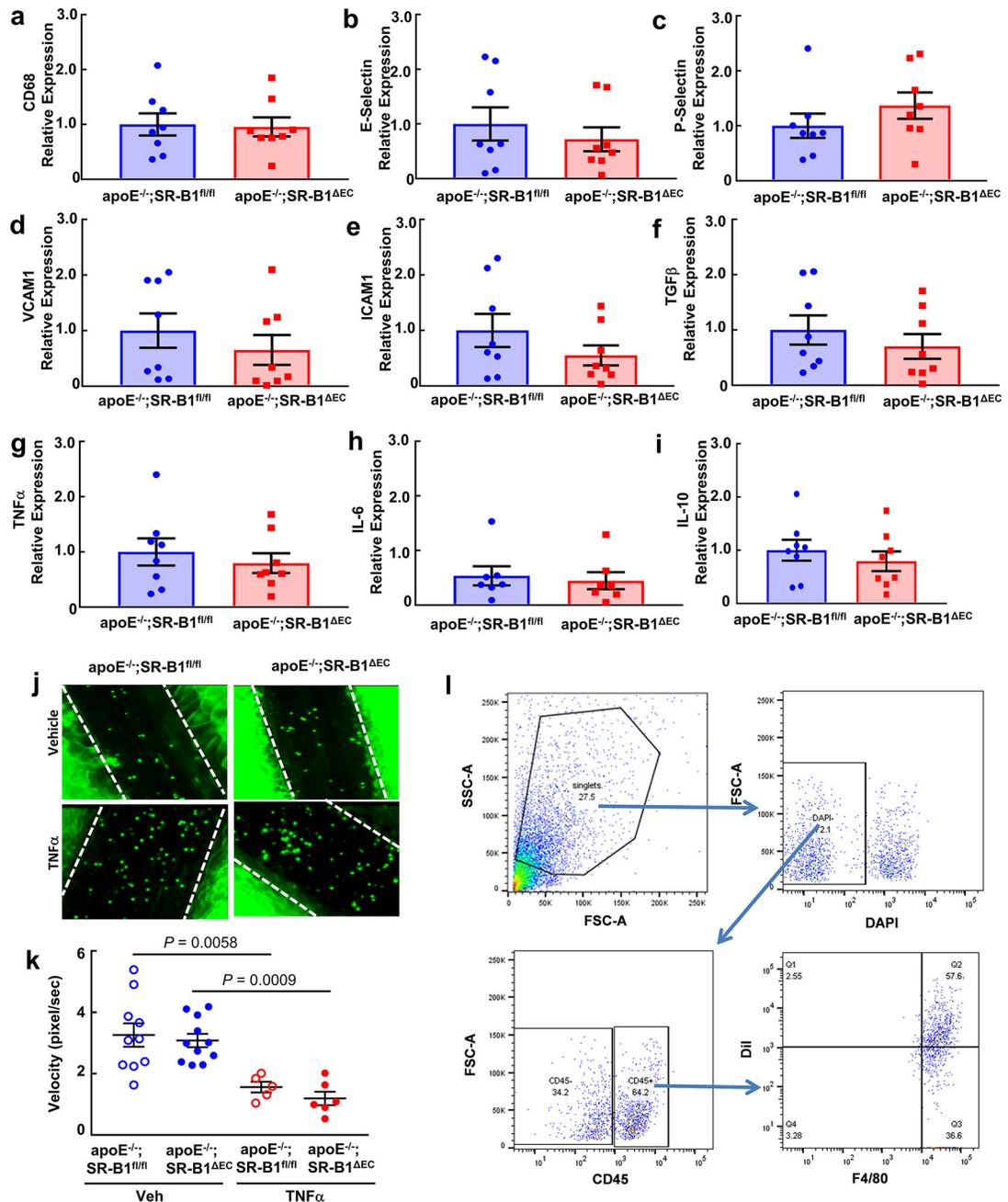
Extended Data Figure 5. Endothelial SR-B1 does not influence vascular inflammation.
a, Quantitative real-time PCR was performed to compare CD68 transcript levels in aortas from apoE$^{-/-}$;SR-B1$^{fl/fl}$ and apoE$^{-/-}$;SR-B1$^{\Delta EC}$ male mice, n=8/group. **b-i**, mRNA abundance was also evaluated for the following genes, using HPRT1 as a housekeeping gene and normalizing expression to CD68 levels: E-selectin (**b**), P-selectin (**c**), VCAM-1 (**d**), ICAM-1 (**e**), TGFβ (**f**), TNFα (**g**), IL-6 (**h**), and IL-10 (**i**), with n=8/group. **j**, Representative still images of leukocyte-endothelial cell adhesion evaluated by intravital microscopy in the mesenteric microcirculation of apoE$^{-/-}$;SR-B1$^{fl/fl}$ and apoE$^{-/-}$;SR-B1$^{\Delta EC}$ male mice administered vehicle (n=10 and 11, respectively) or TNFα (n=5 and 6, respectively). **k**,

...

Summary data for leukocyte velocity in four study groups in j. **l**, Gating strategy for evaluation of CD45+, F4/80+ cell number and DiI-LDL uptake in the aorta. Following digestion of the aorta, all cells were first gated in FSC/SSC according to cell size and granularity. The resulting population was gated according to cell viability using DAPI. DAPI- live cells were gated for positivity for CD45, and CD45+ cells were then gated for positivity for F4/80 and the DiI label. Data are mean±SEM; in k, P values by ANOVA with Dunnett's post-hoc test are shown.
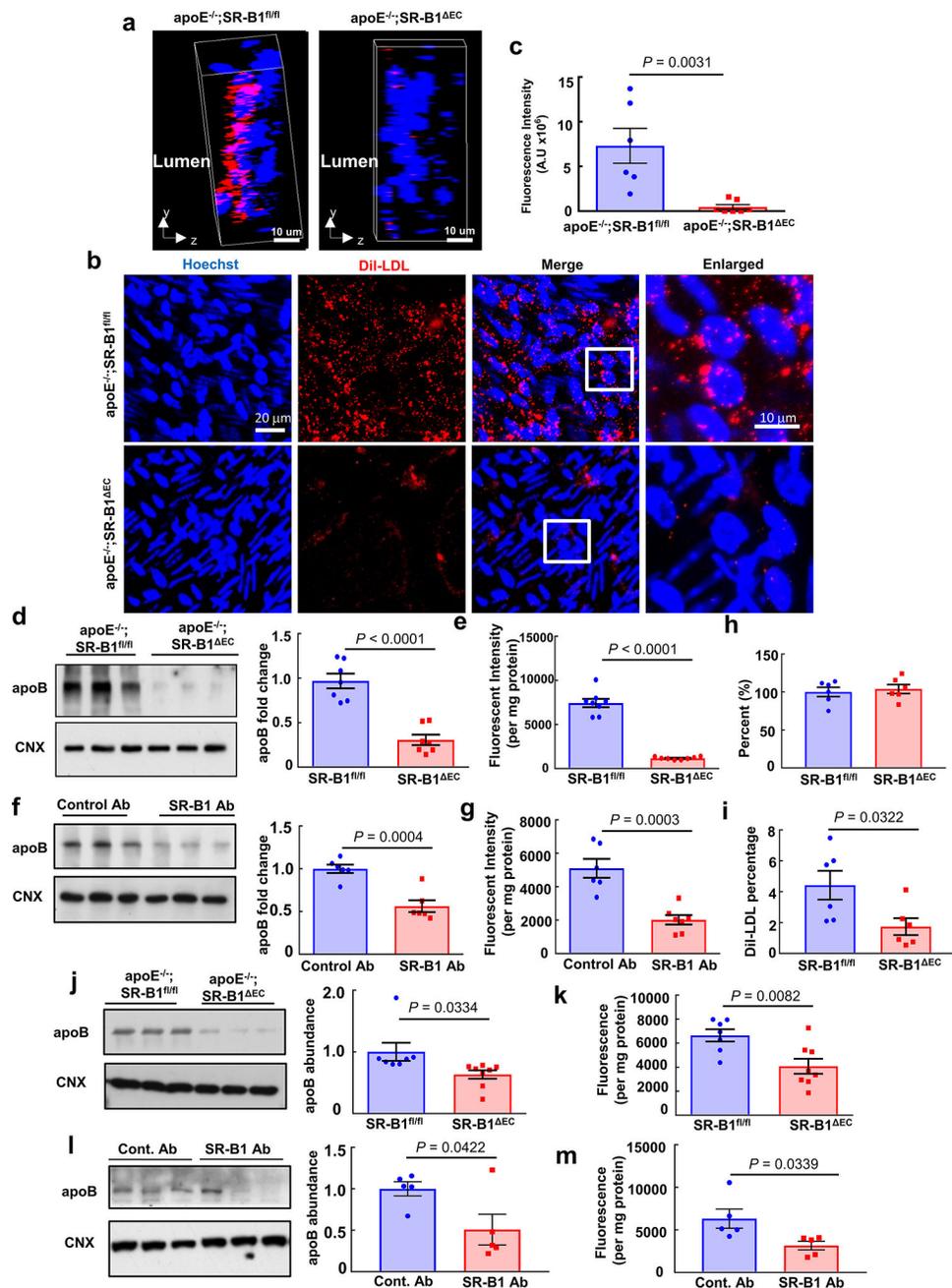
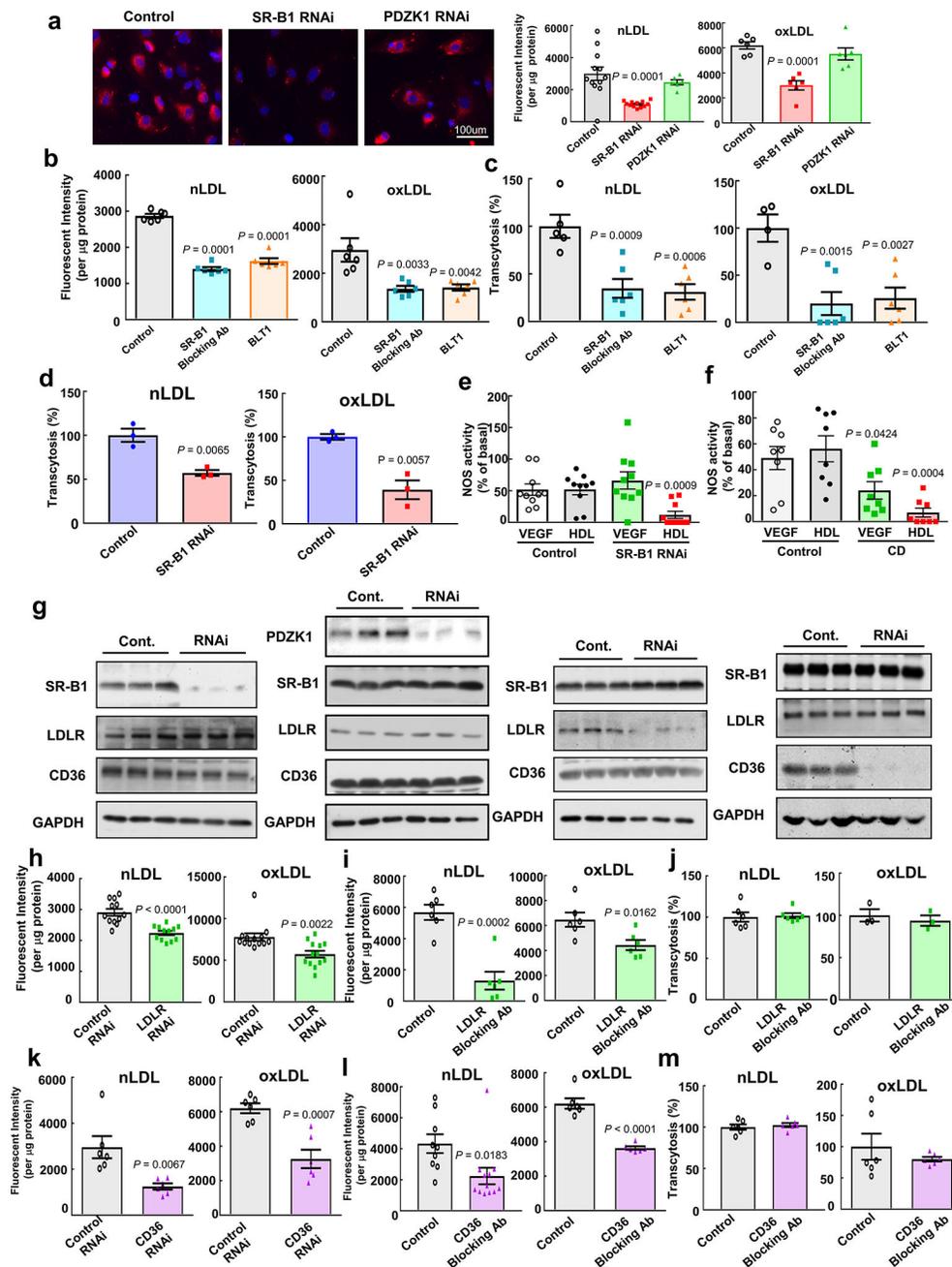**Extended Data Figure 6. Endothelial SR-B1 drives both nLDL and oxLDL delivery into the artery wall.**

a, Three-dimensional depiction of DiI-oxLDL localization determined by confocal fluorescence microscopy of the luminal surface of the ascending aorta of apoE$^{-/-}$;SR-B1$^{fl/fl}$ and apoE$^{-/-}$;SR-B1$^{\Delta EC}$ mice. Lumen is on the left. DiI is shown in red and Hoechst staining of nuclei is shown in blue. **b**, Representative cumulative images of the X-Y plane parallel to the luminal surface. **c**, Summation of dil-oxLDL signal in the superficial ascending aorta. Two areas encompassing at least 100 cells were counted per mouse in 3 mice per group for total n=6/genotype group. **d,e**, Aorta dil-oxLDL uptake. Human apolipoprotein B abundance

(**d**) or Dil fluorescence intensity (**e**) was evaluated in aorta homogenates 4h following IV DiI-oxLDL injection; n=8/group. **f,g**, Using same approaches as in d and e, aorta dil-oxLDL uptake was evaluated in apoE$^{-/-}$ mice treated with control Ab or SR-B1 blocking antibody given IP prior to IV injection of diI-oxLDL (n=6 and 7, respectively). **h**, Quantification of CD45$^+$, F4/80$^+$ macrophages in the aorta (n=6/group). Results are expressed relative to abundance in apoE$^{-/-}$;SR-B1$^{fl/fl}$ control mice. **i**, Dil-oxLDL distribution in CD45$^+$, F4/80$^+$ macrophages in the aorta, n=6/group. **j,k**, Aorta dil-nLDL uptake. Human apolipoprotein B abundance (**j**) or Dil fluorescence intensity (**k**) was evaluated in aorta homogenates 4h following IV DiI-nLDL injection; n=7 and 8, respectively. **l,m**, Using same approaches as in j and k, aorta dil-nLDL uptake was evaluated in apoE$^{-/-}$ mice treated with control Ab or SR-B1 blocking antibody given IP prior to IV injection of diI-nLDL (n=5/group). Left panel in d, f, j and l displays a representative immunoblot with 3 samples per group; Data are mean ±SEM, P values by two-sided Student's t test are shown. See also Videos 1,2.
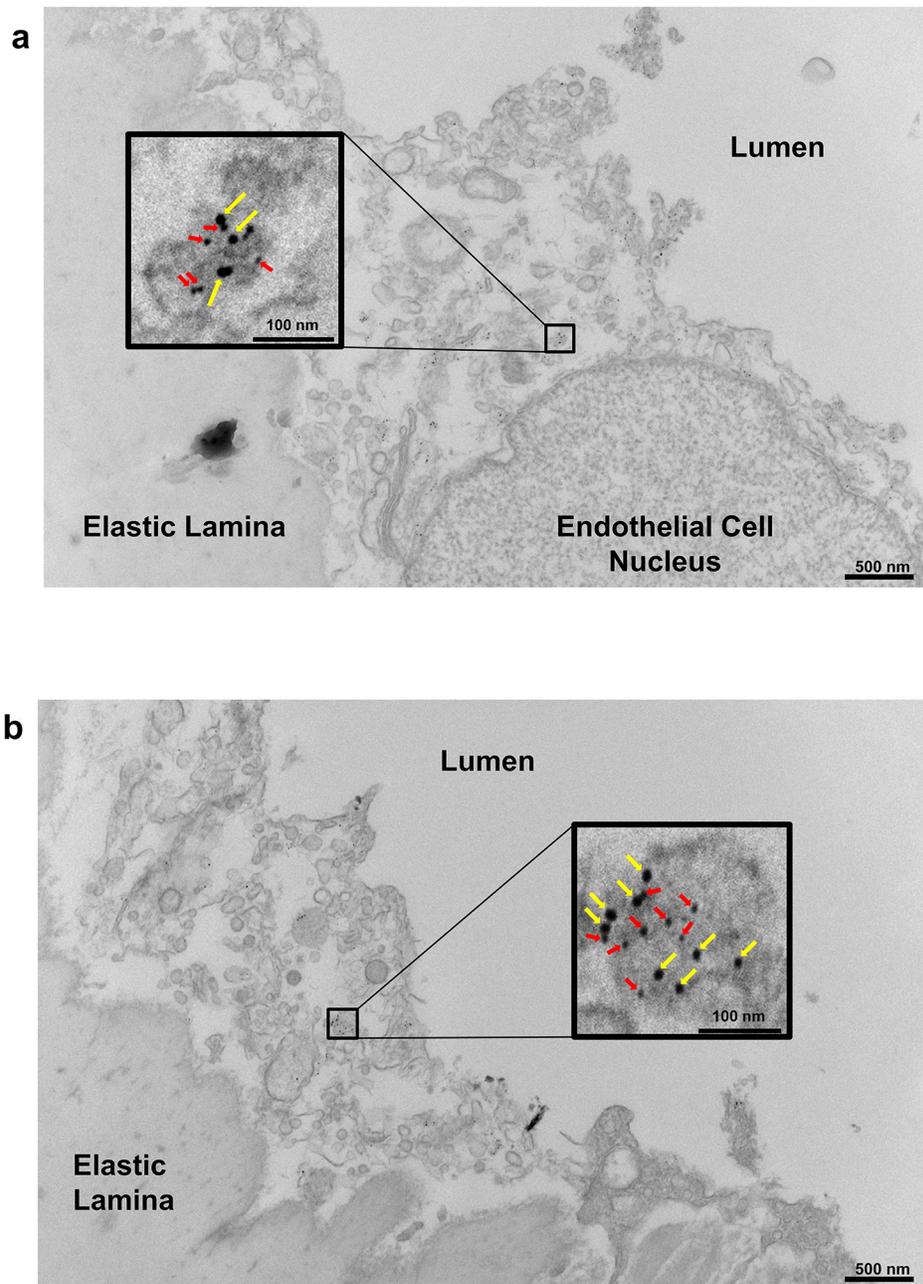
Extended Data Figure 7. Low-power electron micrograph images of LDL-gold and immunogold-labeled SR-B1 in aortic endothelial cells in vivo.
Following intravascular administration in wild-type mice, gold-labeled LDL particles and SR-B1 were localized in aortic endothelial cells by electron microscopy. **a** and **b** display images for two different endothelial cells, each bordered by the lumen and elastic lamina. Shown are the locations of the high-power fields provided in Figure 1n, with LDL-gold (large particles) highlighted by yellow arrows and immunogold-labeled SR-B1 (small particles) highlighted by red arrows.

Extended Data Figure 8. SR-B1 governs endothelial cell LDL transcytosis independent of effects on caveolae function.

a, DiI-nLDL and diI-oxLDL uptake in endothelial cells after RNAi knockdown of SR-B1 or PDZK1. In left panel, diI-oxLDL visualization is shown in red, and DAPI-stained nuclei are in blue. N=6/group. **b,c**, DiI-nLDL and dil-oxLDL uptake (**b**) and transcytosis (**c**) in cells treated with control IgG or SR-B1 blocking antibody or BLT1. N=6/group. **d**, DiI-nLDL and diI-oxLDL transcytosis in endothelial cells after RNAi knockdown of SR-B1. N=3/group. **e,f**, NOS activation by VEGF (100ng/ml) or HDL (20ug/ml) with or without RNAi knockdown of SR-B1 (**e**, n=10/group) or caveolae disruption by methyl-β-cyclodextrin

treatment (**f**, 10mM for 60min, n=8/group). **g**, Abundance of target protein following RNAi knockdown of SR-B1, PDZK1, LDLR or CD36 in HAEC. Findings for 3 samples per condition are shown. In all studies SR-B1, LDLR and CD36 expression were evaluated. **h,i**, DiI-nLDL and diI-oxLDL uptake in cells depleted of LDLR by RNAi (**h**, n=12 for nLDL and 13 for oxLDL) or treated with control versus LDLR blocking antibody (**i**, n=6/group). **j**, DiI-nLDL and diI-oxLDL transcytosis in cells treated with control versus LDLR blocking antibody. N=6 for nLDL and 3 for oxLDL. **k,l**, DiI-nLDL and diI-oxLDL uptake in cells depleted of CD36 by RNAi (**k**, n=6/group) or treated with control versus CD36 blocking antibody (**l**, n=9 and 12 for nLDL and 6 for oxLDL). **m**, DiI-nLDL and diI-oxLDL transcytosis in cells treated with control versus CD36 blocking antibody. N=6/group. Data are mean±SEM, P values by two-sided Student's t test (a-c) or by ANOVA with Dunnett's post-hoc test (d-f, h-I, k-l) are shown.
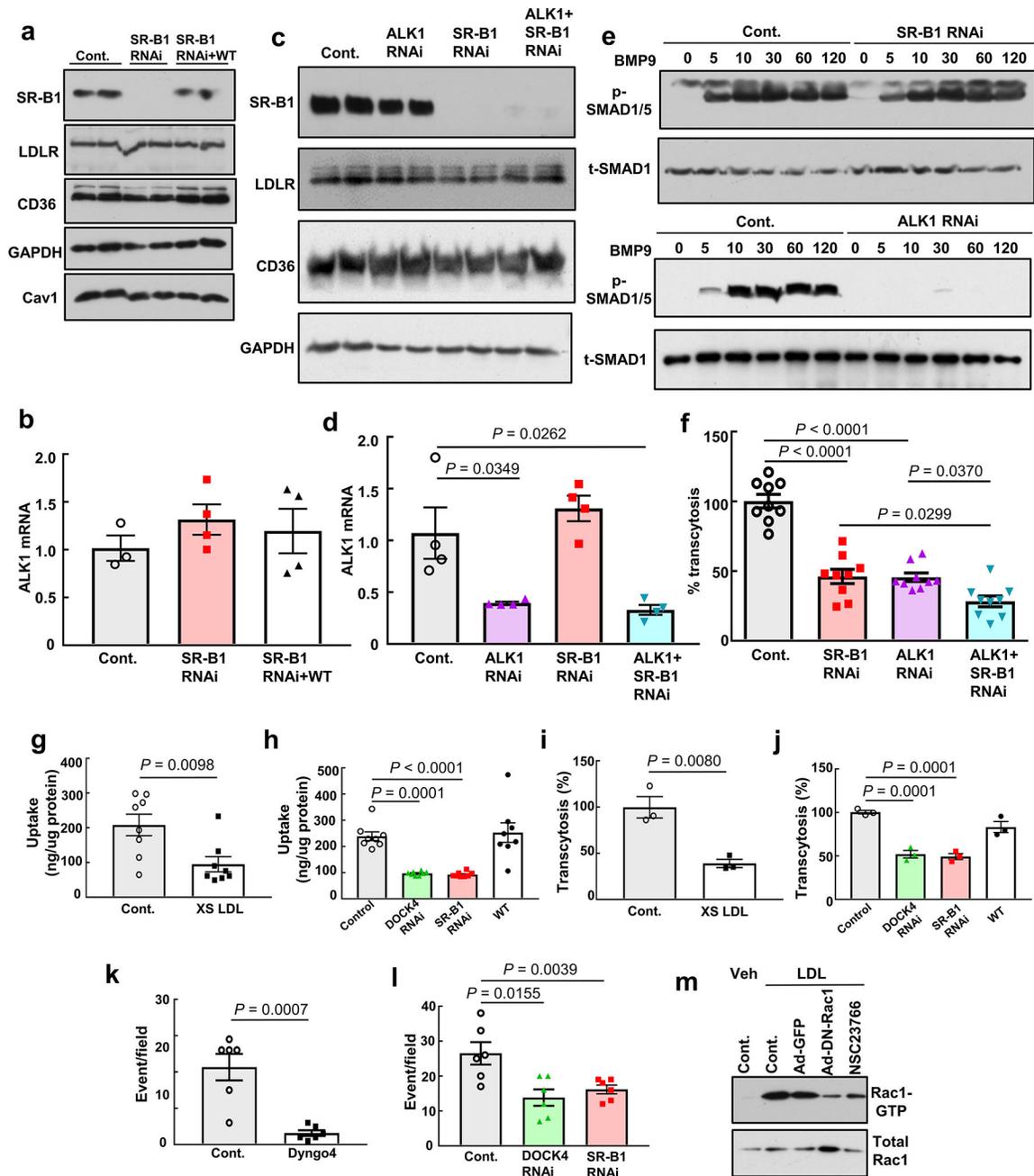
Extended Data Figure 9. Roles of SR-B1, ALK1 and DOCK4 in endothelial cell LDL transcytosis.

a, Abundance of SR-B1, LDLR, and CD36 protein following RNAi knockdown of SR-B1, or following reconstitution of wild-type SR-B1 expression in cells depleted of endogenous receptor. Caveolin-1 (Cav1) expression was also evaluated. Findings for 2 samples per condition are shown. **b**, ALK1 transcript levels in cells manipulated as in a. N=4/group. **c**, Abundance of SR-B1, LDLR, and CD36 protein following RNAi knockdown of ALK1, SR-B1, or ALK1 and SR-B1. Findings for 2 samples per condition are shown. **d**, ALK1 transcript levels in cells manipulated as in c. N=4/group. **e**, SMAD1/5 phosphorylation in

response to BMP9 (10ng/ml, for 0–120 min) following RNAi knockdown of SR-B1 or ALK1. Abundance of SMAD1/5 Ser463/465 phosphorylation and total SMAD1 were evaluated by immunoblotting. **f**, DiI-nLDL transcytosis following RNAi knockdown of ALK1, SR-B1, or ALK1 and SR-B1. N=9/group. **g,h**, nLDL uptake was evaluated using ^{125}I-nLDL in the absence or presence of 50-fold excess unlabeled nLDL (**g**), and **h**, following RNAi knockdown of SR-B1 or DOCK4, or reconstitution of wild-type SR-B1 expression in cells depleted of endogenous receptor. N=8/group. **i,j**, nLDL transcytosis was evaluated using ^{125}I-nLDL in the absence versus presence of 50-fold excess unlabeled nLDL (**i**), and **j**, following manipulation of SR-B1 or DOCK4 expression as in h. N=3/group. **k,l**, nLDL transcytosis was evaluated using total internal reflection fluorescence (TIRF) microscopy in cells treated with Dyngo4A (**k**, 30uM) and **l**, in cells following RNAi knockdown of SR-B1 or DOCK4. N=6/group. **m**, Rac1 activation in response to oxLDL was determined in cells expressing GFP control versus dominant-negative Rac1, and in untreated cells versus cells incubated with the Rac1 inhibitor NSC23766. Data are mean±SEM, P values by ANOVA with Dunnett's posthoc test (d, f, h, j, l) or by two-sided Student's t test (g, i, k) are shown.
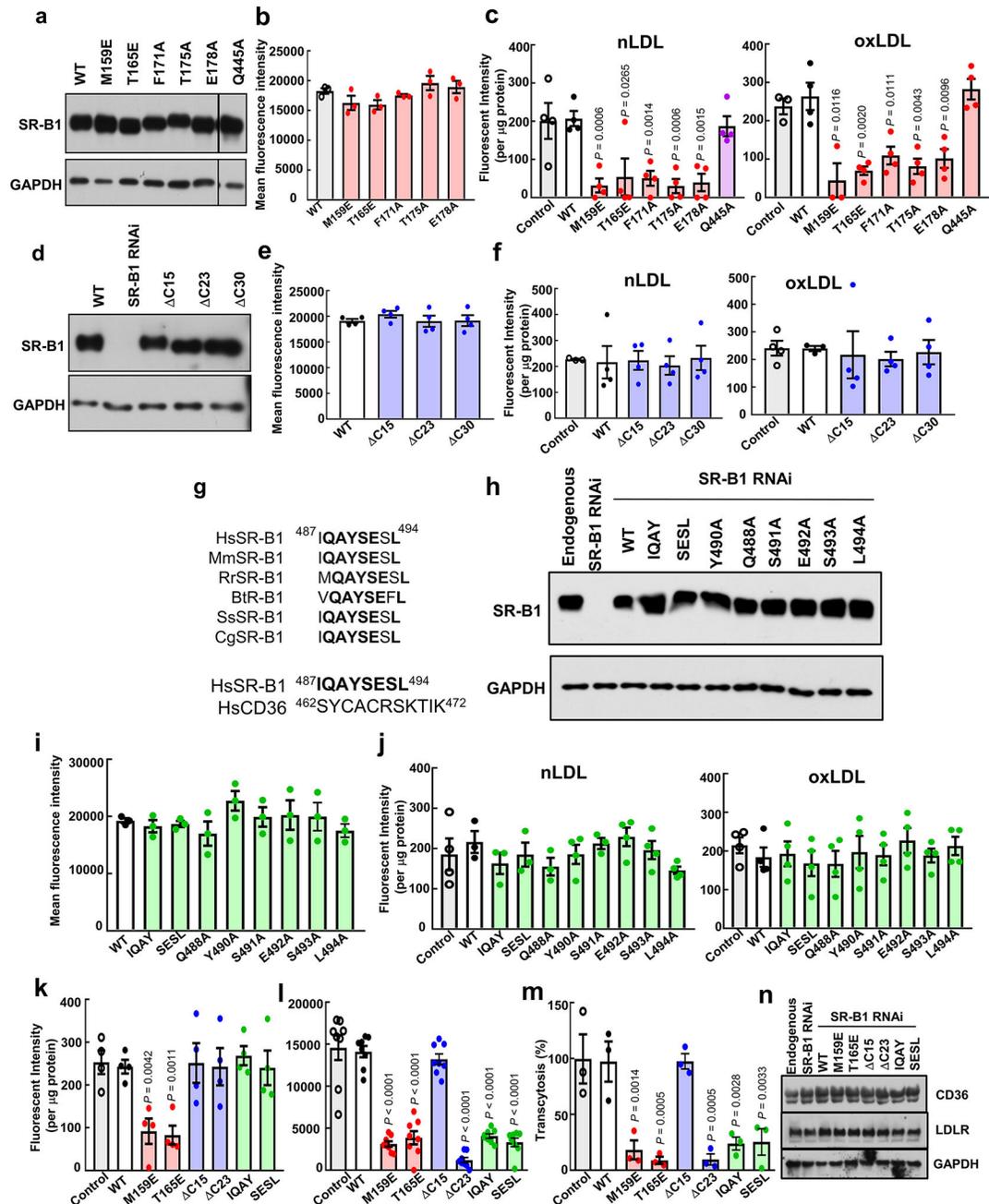
Figure 10. Lentiviral reconstitution of wild-type and mutant SR-B1 expression in human endothelial cells.

a-c, Studies of reconstituted wild-type SR-B1 (WT), extracellular point mutant SR-B1, or SR-B1-Q445A. The extracellular point mutants were: SR-B1-M159E, T165E, F171A, T175A, and E178A. Whole cell lysate abundance (**a**), cell surface abundance (**b**; except for Q445A, which was previously evaluated), and nLDL and oxLDL binding (**c**) were evaluated.

d-f, Studies of reconstituted WT or C-terminal cytoplasmic tail deletion mutant SR-B1. The mutants were: SR-B1-ΔC15 (Δ495–509), ΔC23 (Δ487–509) and ΔC30 (Δ480–509). Whole cell lysate abundance (**d**), cell surface abundance (**e**), and nLDL and oxLDL binding (**f**)

were evaluated. **g**, Upper Panel: Sequence alignment of amino acids in the C-terminal cytoplasmic tail of SR-B1 homologs (residues 487–494) from human (*Homo sapien*, Hs, Q8WTVO, Swiss-Prot), mouse (*Mus musculus*, Mm, Q61009, Swiss- Prot), rat (*Rattus norvegius*, Rr, P97943, Swiss-Prot), bovine (*Bos Taurus*, Bt, O18824, Swiss-Prot), pig (*Sus scrofa*, Ss, Q8SQC1, Swiss-Prot), and Chinese hamster (*Cricetulus griseus*, Cg, Q60417, Swiss-Prot). Fully conserved residues are shown in bold. Lower Panel: Comparison of human SR-B1 residues 487–494 and entire human CD36 C-terminal cytoplasmic tail. Residues of SR-B1 not shared with CD36 are shown in bold. **h-j**, Studies of reconstituted WT or C-terminal cytoplasmic tail substitution mutant SR-B1. The mutants were: SR-B1-IQAY, SESL, Y490A, Q488A, S491A, E492A, S493A, and L494A. Whole cell lysate abundance (**h**), cell surface abundance (**i**), and nLDL and oxLDL binding (**j**) were evaluated. **k-m**, nLDL binding (**k**), uptake (**l**) and transcytosis studies (**m**) were performed with the various mutants shown at an nLDL concentration of 100ug/ml. **n**, Whole cell lysate abundance of CD36 and LDLR was evaluated following reconstitution with the SR-B1 mutants tested in k-m. Data are mean±SEM. For cell surface abundance by flow cytometry, n=3 or 4. For LDL binding, n=4 or 8. For LDL transcytosis, n=3. In c, k-m, P values for comparison with WT by two-sided Student's t test are shown.

Supplementary Material

Refer to Web version on PubMed Central for supplementary material.

ACKNOWLEDGMENTS

REFERENCES

1. Lozano R et al. Global and regional mortality from 235 causes of death for 20 age groups in 1990 and 2010: a systematic analysis for the Global Burden of Disease Study 2010. Lancet 380, 2095–2128 (2012). [PubMed: 23245604]

2. Moore KJ, Sheedy FJ, & Fisher EA Macrophages in atherosclerosis: a dynamic balance. Nat. Rev. Immunol 13, 709–721 (2013). [PubMed: 23995626]

3. Tabas I, Williams KJ, & Boren J Subendothelial lipoprotein retention as the initiating process in atherosclerosis: update and therapeutic implications. Circulation 116, 1832–1844 (2007). [PubMed: 17938300]

4. Gadea G & Blangy A Dock-family exchange factors in cell migration and disease. Eur. J. Cell Biol 93, 466–477 (2014). [PubMed: 25022758]

5. Rosenson RS et al. Cholesterol efflux and atheroprotection: advancing the concept of reverse cholesterol transport. Circulation 125, 1905–1919 (2012). [PubMed: 22508840]

6. Yuhanna IS et al. High-density lipoprotein binding to scavenger receptor-BI activates endothelial nitric oxide synthase. Nat. Med 7, 853–857 (2001). [PubMed: 11433352]

7. Mineo C & Shaul PW Novel biological functions of high-density lipoprotein cholesterol. Circ. Res 111, 1079–1090 (2012). [PubMed: 23023510]

8. Braun A et al. Loss of SR-BI expression leads to the early onset of occlusive atherosclerotic coronary artery disease, spontaneous myocardial infarctions, severe cardiac dysfunction, and premature death in apolipoprotein E-deficient mice. Circ. Res 90, 270–276 (2002). [PubMed: 11861414]

9. Krieger M Scavenger receptor class B type I is a multiligand HDL receptor that influences diverse physiologic systems. J. Clin. Invest 108, 793–797 (2001). [PubMed: 11560945]

10. Armstrong SM et al. A novel assay uncovers an unexpected role for SR-BI in LDL transcytosis. Cardiovasc. Res 108, 268–277 (2015). [PubMed: 26334034]

11. Ishigaki Y et al. Impact of plasma oxidized low-density lipoprotein removal on atherosclerosis. Circulation 118, 75–83 (2008). [PubMed: 18559699]

12. Kato R et al. Transient increase in plasma oxidized LDL during the progression of atherosclerosis in apolipoprotein E knockout mice. Arterioscler. Thromb. Vasc. Biol 29, 33–39 (2009). [PubMed: 18988894]

13. Fung KY et al. SR-BI Mediated Transcytosis of HDL in Brain Microvascular Endothelial Cells Is Independent of Caveolin, Clathrin, and PDZK1. Front Physiol 8, 841 (2017). [PubMed: 29163190]

14. Fernandez-Hernando C et al. Genetic evidence supporting a critical role of endothelial caveolin-1 during the progression of atherosclerosis. Cell Metab 10, 48–54 (2009). [PubMed: 19583953]

15. Pavlides S, Gutierrez-Pajares JL, Iturrieta J, Lisanti MP, & Frank PG Endothelial caveolin-1 plays a major role in the development of atherosclerosis. Cell Tissue Res. 356, 147–157 (2014). [PubMed: 24390341]

16. Sawamura T et al. An endothelial receptor for oxidized low-density lipoprotein. Nature 386, 73–77 (1997). [PubMed: 9052782]

17. Loeffler B et al. Lipoprotein lipase-facilitated uptake of LDL is mediated by the LDL receptor. J. Lipid Res. 48, 288–298 (2007). [PubMed: 17090659]

18. Uittenbogaard A, Shaul PW, Yuhanna IS, Blair A, & Smart EJ High density lipoprotein prevents oxidized low density lipoprotein-induced inhibition of endothelial nitric-oxide synthase localization and activation in caveolae. J. Biol. Chem 275, 11278–11283 (2000). [PubMed: 10753938]

19. Kraehling JR et al. Genome-wide RNAi screen reveals ALK1 mediates LDL uptake and transcytosis in endothelial cells. Nat. Commun 7, 13516 (2016). [PubMed: 27869117]

20. Neculai D et al. Structure of LIMP-2 provides functional insights with implications for SR-BI and CD36. Nature 504, 172–176 (2013). [PubMed: 24162852]

21. Saddar S et al. Scavenger Receptor Class B Type I (SR-BI) is a plasma membrane cholesterol sensor. Circ. Res 112, 140–151 (2012). [PubMed: 23023567]

22. Dieckmann M, Dietrich MF, & Herz J Lipoprotein receptors--an evolutionarily ancient multifunctional receptor family. Biol. Chem 391, 1341–1363 (2010). [PubMed: 20868222]

23. Yajnik V et al. DOCK4, a GTPase activator, is disrupted during tumorigenesis. Cell 112, 673–684 (2003). [PubMed: 12628187]

24. Kawada K et al. Cell migration is regulated by platelet-derived growth factor receptor endocytosis. Mol. Cell Biol. 29, 4508–4518 (2009). [PubMed: 19528233]

25. Stocker R & Keaney JF Jr. Role of oxidative modifications in atherosclerosis. Physiol Rev. 84, 1381–1478 (2004). [PubMed: 15383655]

26. Kwak BR et al. Biomechanical factors in atherosclerosis: mechanisms and clinical implications. Eur. Heart J. 35, 3013–3020d (2014). [PubMed: 25230814]

27. Tabas I, Garcia-Cardena G, & Owens GK Recent insights into the cellular biology of atherosclerosis. J. Cell Biol. 209, 13–22 (2015). [PubMed: 25869663]

28. Vaisman BL et al. Endothelial Expression of Scavenger Receptor Class B, Type I Protects against Development of Atherosclerosis in Mice. Biomed. Res. Int 2015, 607120 (2015). [PubMed: 26504816]

29. Tang Y, Harrington A, Yang X, Friesel RE, & Liaw L The contribution of the Tie2+ lineage to primitive and definitive hematopoietic cells. Genesis. 48, 563–567 (2010). [PubMed: 20645309]

30. Wang J et al. Relative roles of ABCG5/ABCG8 in liver and intestine. J. Lipid Res. 56, 319–330 (2015). [PubMed: 25378657]

31. Warming S, Costantino N, Court DL, Jenkins NA, & Copeland NGSimple and highly efficient BAC recombineering using galK selection. Nucleic Acids Res. 33, e36 (2005). [PubMed: 15731329]

32. Tanigaki K et al. Endothelial Fcgamma Receptor IIB Activation Blunts Insulin Delivery to Skeletal Muscle to Cause Insulin Resistance in Mice. Diabetes 65, 1996–2005 (2016). [PubMed: 27207525]

33. Huang L, Fan B, Ma A, Shaul PW, & Zhu H Inhibition of ABCA1 protein degradation promotes HDL cholesterol efflux capacity and RCT and reduces atherosclerosis in mice. J. Lipid Res. 56, 986–997 (2015). [PubMed: 25761370]

34. Ouimet M et al. MicroRNA-33-dependent regulation of macrophage metabolism directs immune cell polarization in atherosclerosis. J. Clin. Invest 125, 4334–4348 (2015). [PubMed: 26517695]

35. Umetani M et al. The cholesterol metabolite 27-hydroxycholesterol promotes atherosclerosis via proinflammatory processes mediated by estrogen receptor alpha. Cell Metab 20, 172–182 (2014). [PubMed: 24954418]

36. Graesser D et al. Altered vascular permeability and early onset of experimental autoimmune encephalomyelitis in PECAM-1-deficient mice. J. Clin. Invest 109, 383–392 (2002). [PubMed: 11827998]

37. Rong S et al. Expression of SREBP-1c Requires SREBP-2-mediated Generation of a Sterol Ligand for LXR in Livers of Mice. Elife. 6, (2017).

38. Stephan ZF & Yurachek EC Rapid fluorometric assay of LDL receptor activity by DiI-labeled LDL. J. Lipid Res. 34, 325–330 (1993). [PubMed: 8381454]

39. Lim HY et al. Lymphatic vessels are essential for the removal of cholesterol from peripheral tissues by SR-BI-mediated transport of HDL. Cell Metab 17, 671–684 (2013). [PubMed: 23663736]

40. Jia JM et al. Control of cerebral ischemia with magnetic nanoparticles. Nat. Methods 14, 160–166 (2017). [PubMed: 27941784]

41. Duivenvoorden R et al. A statin-loaded reconstituted high-density lipoprotein nanoparticle inhibits atherosclerotic plaque inflammation. Nat. Commun 5, 3065 (2014). [PubMed: 24445279]

42. Handley DA, Arbeeny CM, Witte LD, & Chien S Colloidal gold--low density lipoprotein conjugates as membrane receptor probes. Proc. Natl. Acad. Sci. U. S. A 78, 368–371 (1981). [PubMed: 6264440]

43. Michaely P, Li WP, Anderson RG, Cohen JC, & Hobbs HH The modular adaptor protein ARH is required for low density lipoprotein (LDL) binding and internalization but not for LDL receptor clustering in coated pits. J. Biol. Chem 279, 34023–34031 (2004). [PubMed: 15166224]

44. Ganesan LP et al. Scavenger receptor B1, the HDL receptor, is expressed abundantly in liver sinusoidal endothelial cells. Sci. Rep 6, 20646 (2016). [PubMed: 26865459]

45. Nieland TJ, Penman M, Dori L, Krieger M, & Kirchhausen T Discovery of chemical inhibitors of the selective transfer of lipids mediated by the HDL receptor SR-BI. Proc. Natl. Acad. Sci U. S. A 99, 15422–15427 (2002). [PubMed: 12438696]

46. Tanigaki K et al. Hyposialylated IgG activates endothelial IgG receptor FcgammaRIIB to promote obesity-induced insulin resistance. J. Clin. Invest 128, 309–322 (2018). [PubMed: 29202472]

47. Connelly MA et al. Analysis of chimeric receptors shows that multiple distinct functional activities of scavenger receptor, class B, type I (SR-BI), are localized to the extracellular receptor domain. Biochemistry (Mosc. 40, 5249–5259 (2001).

48. Trudgian DC et al. CPFP: a central proteomics facilities pipeline. Bioinformatics. 26, 1131–1132 (2010). [PubMed: 20189941]

49. Trudgian DC et al. Comparative evaluation of label-free SINQ normalized spectral index quantitation in the central proteomics facilities pipeline. Proteomics. 11, 2790–2797 (2011). [PubMed: 21656681]

50. Kim D, Langmead B, & Salzberg SL HISAT: a fast spliced aligner with low memory requirements. Nat. Methods 12, 357–360 (2015). [PubMed: 25751142]

51. Trapnell C et al. Transcript assembly and quantification by RNA-Seq reveals unannotated transcripts and isoform switching during cell differentiation. Nat. Biotechnol 28, 511–515 (2010). [PubMed: 20436464]

52. Armstrong SM et al. Co-regulation of transcellular and paracellular leak across microvascular endothelium by dynamin and Rac. Am. J. Pathol 180, 1308–1323 (2012). [PubMed: 22203054]

53. Baumer Y, Spindler V, Werthmann RC, Bunemann M, & Waschke J Role of Rac 1 and cAMP in endothelial barrier stabilization and thrombin-induced barrier breakdown. J. Cell Physiol 220, 716–726 (2009). [PubMed: 19472214]
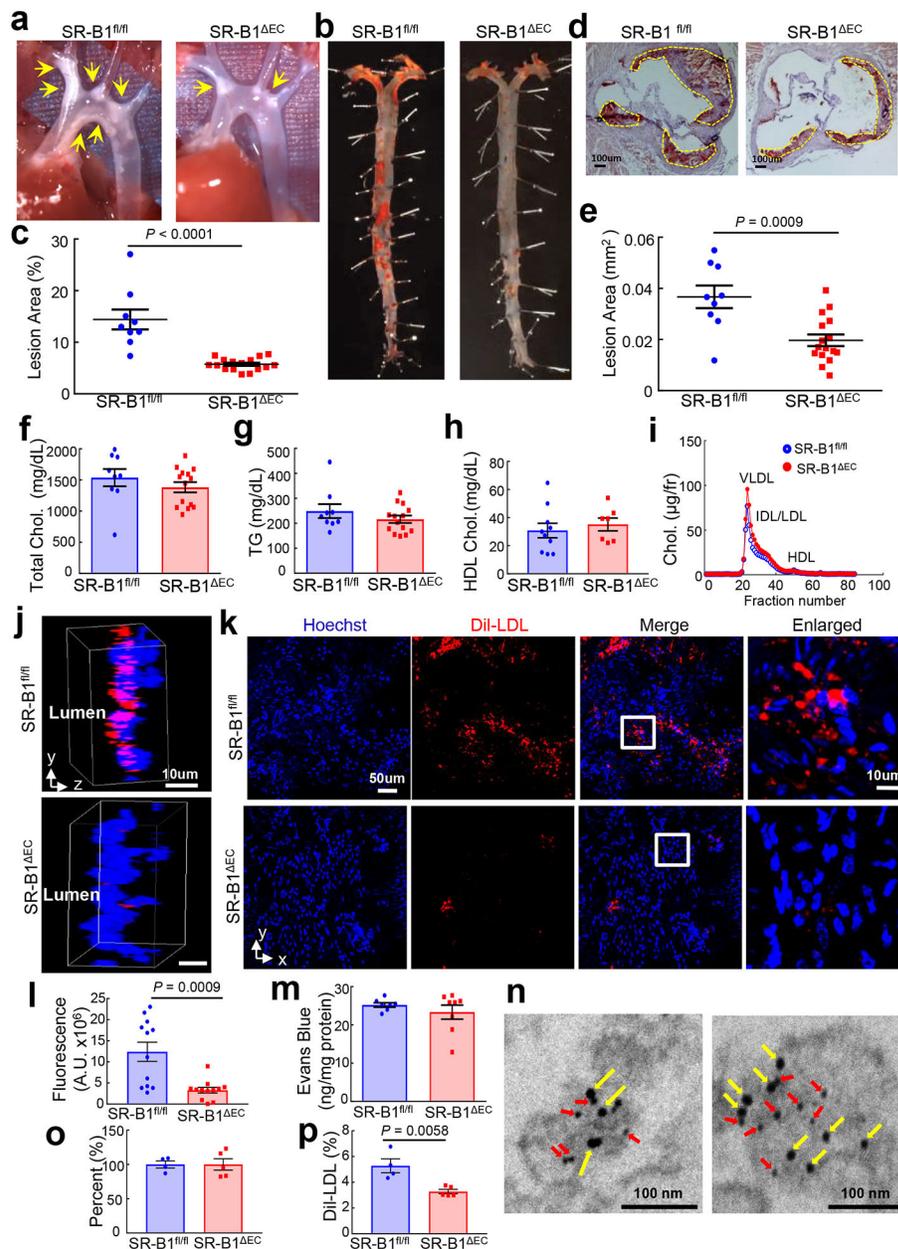
Figure 1. Endothelial SR-B1 promotes atherosclerosis by driving LDL delivery into the artery wall and uptake by artery wall macrophages.

a, Representative in situ aortic arch images of atherosclerotic plaque (yellow arrows) in male apoE$^{-/-}$;SR-B1$^{fl/fl}$ and apoE$^{-/-}$;SR-B1 ^{EC} mice. **b**, Representative lipid-stained *en face* images of aortas. **c**, Quantitation of lesion areas in *en face* aortas (percent of total surface area); n=9 and 16, respectively. **d**, Representative lipid/hematoxylin-stained aortic root sections (lesions outlined by yellow dashed line, magnification 40X), **e**, Quantitation of lesion areas in aortic root sections; n=9 and 16, respectively. **f-h**, Plasma total cholesterol (**f**) and triglyceride (**g**, n=9 and 14, respectively), and HDL cholesterol (**h**, n=7 and 9, respectively). **i**, Representative lipoprotein profiles. **j**, Three-dimensional depiction of Dil-nLDL localization determined by confocal fluorescence microscopy of the luminal surface

of the ascending aorta. Lumen is on the left. DiI is shown in red and Hoechst staining of nuclei is shown in blue. **k**, Representative cumulative images of the X-Y plane parallel to the luminal surface. **l**, Summation of dil-nLDL signal in the superficial ascending aorta. Four areas encompassing at least 100 cells were counted per mouse in 3 mice per group for total n=12/genotype group. **m**, Evaluation of aorta endothelial permeability by quantification of Evans blue dye incorporation (n=7 and 8, respectively). **n**, Gold-labeled LDL (large particles, yellow arrows) and immunogold-labeled SR-B1 (small particles, red arrows) are colocalized in endothelial cell intracellular vesicles in vivo. Representative images from two different endothelial cells are shown. **o**, Quantification of CD45^{+}, F4/80^{+} macrophages in the aorta (n=4 and 5, respectively). Results are expressed relative to abundance in apoE^{−/−};SR-B1^{fl/fl} control mice. **p**, Dil-nLDL distribution in CD45^{+}, F4/80^{+} macrophages in the aorta; n=4 and 5, respectively. Data are mean±SEM, P values by two-sided Student's t test are shown. See also Extended Data Figs. 1a–i, 2–4, 6 and 7.
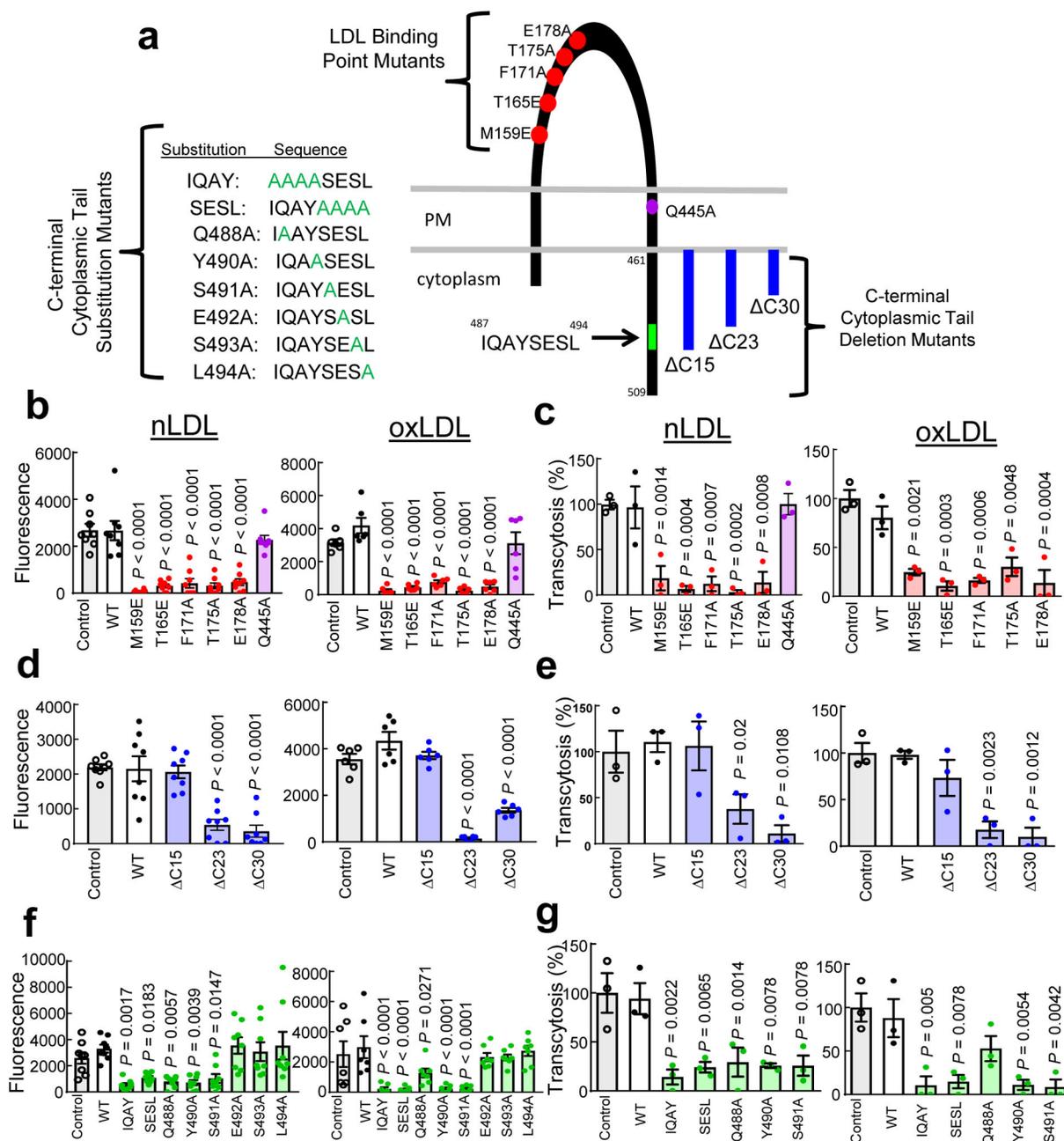
Figure 2. SR-B1 mediation of endothelial cell LDL uptake and transcytosis requires LDL binding to SR-B1 and an 8 amino acid cytoplasmic domain.

a, Schematic of mutant forms of SR-B1 studied by reconstitution in HAEC. **b,c**, nLDL and oxLDL uptake (**b**, n=8 for nLDL and 6 for oxLDL) and transcytosis (**c**, n=3) by wild-type (WT) SR-B1 versus LDL binding point mutants or SR-BI-Q445A. **d,e**, nLDL and oxLDL uptake (**d**, n=8 for nLDL and 6 for oxLDL) and transcytosis (**e**, n=3) by WT SR-B1 versus C-terminal cytoplasmic tail deletion mutants. **f,g**, nLDL and oxLDL uptake (**f**, n=6 or 8) and transcytosis (**g**, n=3) by WT SR-B1 versus C-terminal cytoplasmic tail substitution mutants.

Data are mean±SEM, P values by ANOVA with Dunnett's post-hoc testing are shown. See also Extended Data Fig. 10.
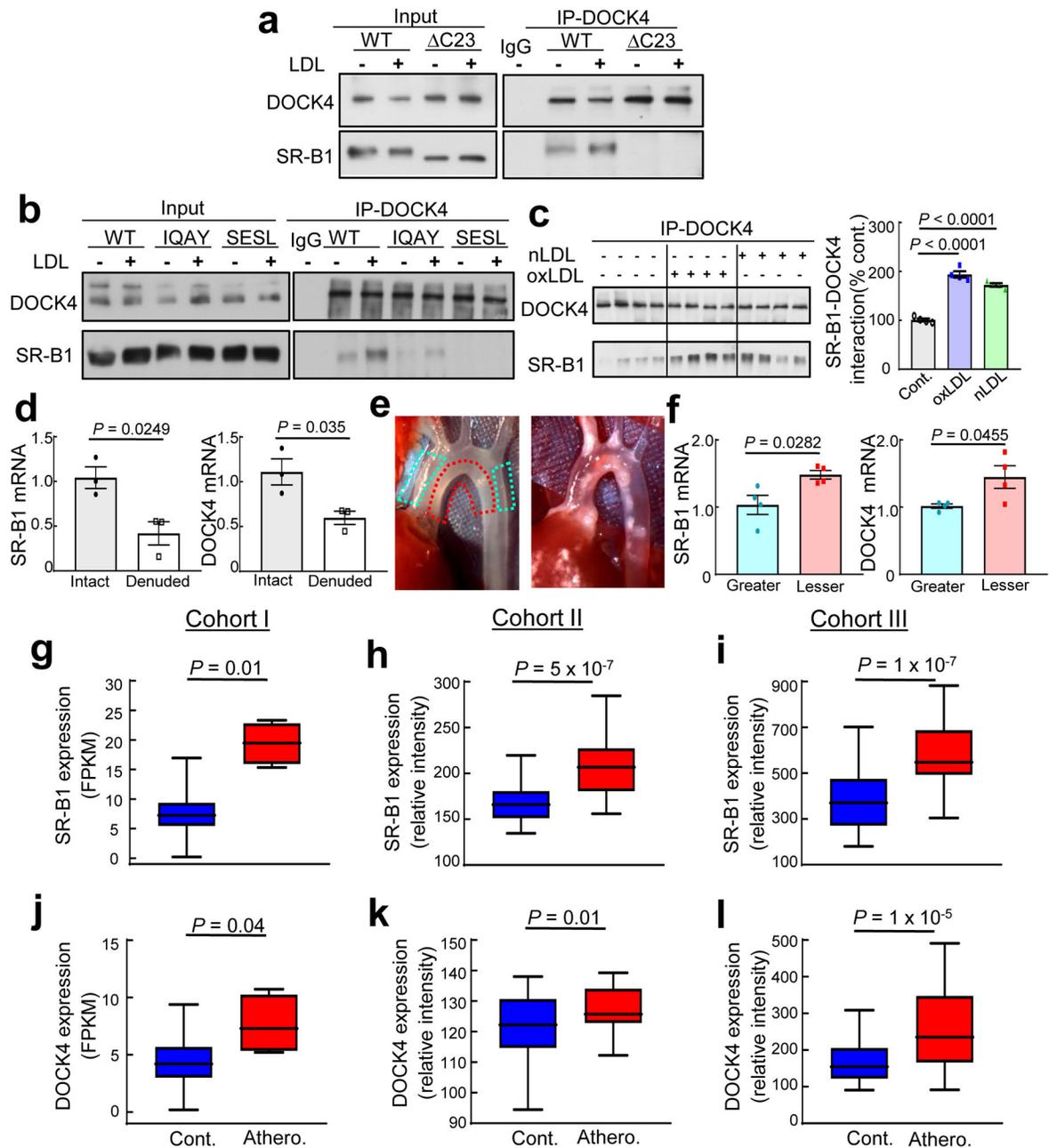
Figure 3. SR-B1 dynamically interacts with DOCK4 in endothelial cells, and their expression is increased in atherosclerosis-prone regions of mouse aorta prior to lesion formation, and in human atherosclerotic versus normal arteries.

a, HAEC expressing His-tagged wild-type SR-B1 or SR-B1- C23 were treated with vehicle or oxLDL, DOCK4 was immunoprecipitated (IP), and immunoblotting was done for DOCK4 and SR-B1. First IP lane shows IP done with unrelated IgG. **b**, Same experiment was performed in HAEC expressing His-tagged wild-type SR-B1, SR-B1-IQAY or SR-B1-SESL. **c**, HAEC reconstituted with His-tagged wild-type SR-B1 were treated with nLDL or oxLDL, DOCK4 was IP'd and immunoblotting was done for DOCK4 and SR-B1. Summary

data are for n=4 per group; P values by ANOVA with Dunnett's post-hoc testing are shown. **d**, SR-B1 and DOCK4 expression were evaluated in intact versus endothelium-denuded mouse aorta by Q-RT-PCR, n=3 arteries per group. **e**, Left panel: In situ image of aortic arch from a wild-type, atherosclerosis-free mouse, depicting regions of greater curvature (blue hashed line) and lesser curvature (red hashed line) sampled for experiment in f. Right panel: In situ image of aortic arch from apoE$^{-/-}$ mouse with atherosclerotic lesions absent in greater curvature and present in lesser curvature. **f**, SR-B1 and DOCK4 expression were evaluated in greater and lesser curvature samples by Q-RT-PCR, n=4 arteries per group. **g-l**, Employing three separate patient cohorts and independent strategies for analyses, SR-B1 (**g-i**) and DOCK4 expression (**j-l**) were compared in human atherosclerotic versus control arteries. Cohorts I, II and III contained n=4 and 207, 40 and 40, and 32 and 32, respectively. Data are mean±SEM; in d and f, P values by two-sided Student's t test are shown; in g-l, data are presented as box-and-whisker plots, with the central lines denoting medians, edges of the box representing upper and lower quartiles, and whiskers showing minimum and maximum values after excluding outliers outside 1.5 times the interquartile range.
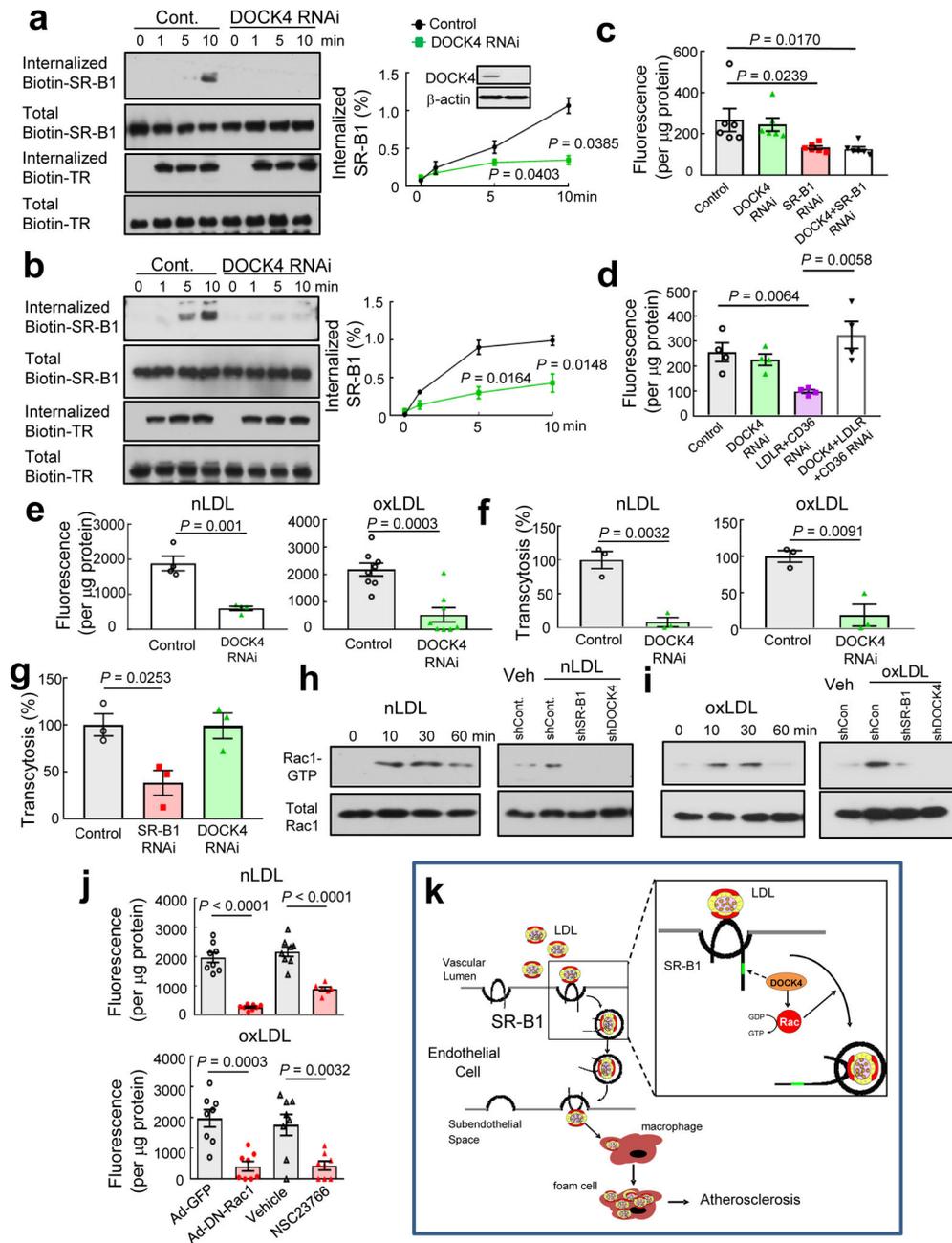
Figure 4. DOCK4 mediates endothelial cell LDL uptake and transcytosis by internalizing SR-B1 and coupling the receptor to Rac1.

a,b, The internalization of biotinylated SR-B1 and transferrin receptor (TR) was evaluated following warming from 4°C to 37°C in nLDL- (**a**) or oxLDL-treated (**b**) endothelial cells with normal versus decreased DOCK4 expression. In a-b, n=3/condition and P values by two-sided Student's t test are shown. **c,d**, DiI-nLDL binding to endothelial cells was evaluated in the presence versus absence of DOCK4 in cells expressing versus deficient in SR-B1 (**c**, n=6) or LDLR and CD36 (**d**, n=4). In c-d, P values by ANOVA with Dunnett's post-hoc testing are shown. **e,f**, nLDL and oxLDL uptake (**e**, n=3 for nLDL and n=8 for

oxLDL) and transcytosis (**f**, n=3) in cells with normal versus decreased DOCK4 expression. **g**, HDL transcytosis in cells with normal versus decreased expression of SR-B1 or DOCK4, n=3. **h,i**, Rac1 is activated by nLDL (**h**) or oxLDL (**i**) via SR-B1 and DOCK4 in endothelial cells. Left panel: Cells were treated with LDL for 0–60 min and Rac1 activity was determined. Right panel: Rac1 activation in response to LDL was evaluated in cells expressing or lacking SR-B1 or DOCK4. **j**, Rac1 activation is required for SR-B1-mediated nLDL or oxLDL uptake in endothelial cells. Cells were transfected with GFP control versus dominant-negative Rac1, or treated with vehicle versus the Rac1 inhibitor NSC23766; n=8. Data are mean±SEM, in e-g and j, P values by two-sided Student's t test are shown. See also Extended Data Fig. 9g–m. **k**, Summary scheme: SR-B1 transports LDL across the endothelial cell monolayer and thereby governs the accumulation of LDL by arterial wall macrophages, which become foam cells and atherosclerotic lesion development ensues. The transcytosis of LDL across the endothelial cell monolayer requires an 8 amino acid cytoplasmic domain of SR-B1, which recruits DOCK4, and DOCK4 promotes SR-B1 internalization and LDL transport by coupling LDL binding to SR-B1 with Rac1 activation.